NATIONAL ADVISORY COMMITTEE FOR AERONAUTICS

TECHNICAL NOTE 3342

EXPERIMENTAL DETERMINATION OF BOUNDARY-LAYER TRANSITION ON A BODY OF REVOLUTION AT M = 3.5

By James R. Jedlicka, Max E. Wilkins, and Alvin Seiff

SUMMARY

Transition tests were made in free-flight on a slender body of revolution at a Mach number of 3.5, wall to free-stream temperature ratio of unity, and with a noiseless and zero-turbulence air stream. The parameter which was varied was surface roughness.

Of the several surfaces tested, two were found that were smooth enough to allow fully laminar flow over the test body to a Reynolds number of 11 million. With surfaces smooth enough to give fully laminar flow near zero angle of attack, transition moved forward rapidly on the sheltered side with increasing angle of attack beginning at 1°. A theoretical study of this effect in terms of the pressure rise along streamlines indicated that sheltered-side transition could be delayed to much larger angles of attack by use of bodies having low fineness ratios and long nose sections. The transition point was found to be time dependent and to fluctuate over a sometimes-extensive region. Unsteadiness of the boundary-layer flow was also evidenced by the occurrence of brief bursts of turbulence. Transition due to roughness and adverse pressure gradient occurred even though the tests were in the region of theoretical infinite laminar stability to small disturbances. This is probably not inconsistent with the theory which does not consider disturbances of the magnitude here involved.

INTRODUCTION

The cooling requirements of an aircraft flying at high supersonic speed will be determined to a large extent by the nature of the boundary-layer flow, that is, the extent to which it is laminar or turbulent. Since, in some cases, aerodynamic heating may be the governing

consideration in design, knowledge of the transition point is of primary importance. Even when heating is not an important consideration, the extent of laminar flow can have an important bearing on the efficiency of flight.

At subsonic speeds, the transition point has been estimated mainly from flight experience. The limited amount of flight experience at supersonic speeds has made it necessary to rely on wind-tunnel data. Unfortunately these data are conflicting and strongly reflect the stream imperfections of the wind tunnels in which they were obtained. The effects of the variables involved have not, for the most part, been separated.

A few experiments have indicated the possibility of long laminar runs under "cold-wall" conditions at Mach numbers above 1. The longest laminar run, laminar to a Reynolds number of 90 million, was reported by Sternberg (ref. 1) from free-flight tests with a V-2 rocket. In wind tunnels, the longest laminar run reported is 28 million in the presence of a cold wall and favorable pressure gradient (ref. 2).

The present tests were originally undertaken to study the effects of surface roughness on transition and also to investigate the lengths of laminar run that might be obtained under favorable conditions. Although pressure-gradient effects were not intended for study, they nevertheless occurred, due mainly to angle of attack, and, in some cases overshadowed the effects of surface roughness. The tests were conducted in free flight through still air, thus eliminating the troublesome effects of stream imperfections. The temperature conditions of the test were the cold-wall conditions favorable to long runs of laminar flow. Specifically, the wall to free-stream temperature ratio was 1.0 and fell within the region of infinite laminar stability to small disturbances as calculated by Van Driest (ref. 3). The tests were conducted in the Ames supersonic free-flight wind tunnel at a Mach number of 3.5 and at body-length Reynolds numbers up to 24 million. The experimental work was done between March 1952 and June 1953.

NOTATION

c	specific heat of model, Btu/slug $^{\circ}F$
C_f	local skin-friction coefficient, dimensionless
c_p	specific heat of air at constant pressure, Btu/slug $^{\circ}F$
C_p	pressure coefficient, $\frac{p-p_o}{q_o}$, dimensionless
d	body diameter, ft

h	height of roughness, ft (unless otherwise noted)
h	local convective heat-transfer coefficient (used in Appendix), Btu/sec ft^2 ^oF
$\bar{h}$	average convective heat-transfer coefficient, Btu/sec ft^2 ^oF
k	thermal conductivity of model, Btu ft/sec ft^2 ^oF
l	over-all body length, ft
M	Mach number, dimensionless
p	local static pressure, lb/ft^2
p_o	free-stream static pressure, lb/ft^2
$\frac{\Delta p}{q_o}$	pressure-rise coefficient (difference between the pressure coefficient at a particular body station and the minimum pressure coefficient), dimensionless
$\left(\frac{\Delta p}{q_o}\right)_{crit}$	critical-pressure-rise coefficient (the value of pressure-rise coefficient above which transition due to pressure rise will occur), dimensionless
q_o	free-stream dynamic pressure, lb/ft^2
r	local body radius, ft
R	Reynolds number based on free-stream properties and length of run, dimensionless
R_l	Reynolds number based on over-all body length, dimensionless
R_T	instantaneous transition Reynolds number, dimensionless
$(R_T)_{av}$	arithmetic average of the instantaneous transition Reynolds numbers
S_b	body cross section at any station, ft^2
S_w	body wetted area ahead of any station, ft^2
t	time, sec
T	absolute temperature, ^oF abs

T_i initial body temperature, °F abs

T_o free-stream static temperature, °F abs

T_r boundary-layer recovery temperature, °F abs

T_w wall temperature, °F abs.

u air velocity, ft/sec

x distance along axis of symmetry from model tip, ft

x_n length of body nose from tip to point of tangency to cylindrical section, ft

y radial distance, measured perpendicular to model axis, ft

α angle of attack, deg

β half angle of cone which is tangent to ogive at model tip, deg

δ laminar boundary-layer thickness (distance normal to body surface at which velocity is 0.995 of the inviscid flow velocity), ft

θ meridian angle of model, measured from windward side, deg

ρ air density, slugs/ft^3

ρ_m density of model, slugs/ft^3

DESCRIPTION OF TESTS

Experimental Method and Test Conditions

This investigation was conducted in free flight at small scale by launching test models through still air from a caliber 50 smooth-bore gun at 4000 feet per second. The models, figures 1 and 2, were fin-stabilized bodies of revolution 6 inches long with a fineness ratio of 30. They were made of aluminum alloy, 75S-T6. They were launched from the gun with the aid of a plastic sabot, figures 2(b) and 2(c). In flight, they passed through a series of high-speed shadowgraph stations located between 40 and 55 feet from the gun, producing a total of seven shadowgraph pictures, four in the horizontal plane and three in the vertical plane. Seventy feet from the gun, the models were

destroyed on impact in a model catcher. Additional description of the equipment and technique used can be found in reference 4.

The tests were conducted at a nominal Mach number of 3.5 and at length Reynolds numbers of 12 and 24 million. The test Reynolds number was varied by changing the static pressure in the test section within the limits of 1 atmosphere and 2 atmospheres absolute. At all pressures the free-stream air in the test section was at rest. The model skin temperature, which is known to be a significant test condition for boundary-layer transition, could not be measured but was estimated according to the method given in the Appendix. The surface temperature rise with laminar boundary layer after 50 feet of flight through air at 1 atmosphere static pressure was found to be negligible except within a few hundredths of an inch of the model tip. (This is understandable when it is considered that the time of flight is only 12.5 milliseconds). At the mathematical tip, a temperature rise approaching 300° F was found to be possible. Therefore, the wall to free-stream static temperature ratio is 1.0 over practically all the body and about 1.5 at the tip; in any case the ratio is always less than 1.85, the temperature ratio below which infinite laminar stability theoretically occurs according to the calculations of reference 3.

Methods of Measuring Transition Point, Angle of Attack, and Surface Roughness

The data obtained in these tests were measurements of transition point, angle of attack, and surface roughness. The methods of measuring these quantities will be described in this section.

Transition point.- Transition data were obtained from shadowgraph pictures. Those in figure 3 are typical. Transition to turbulent flow was identified by the appearance of eddies at the model edge, the obliteration of the diffraction line which occurs with a thin laminar boundary layer or with no flow, and the occurrence of steep Mach waves in the flow outside the boundary layer (caused by the irregular contour of the turbulent flow). Transition so defined is indicated by the arrows in figure 3. Evidence that transition determined optically coincides with transition determined by other means, such as a boundary-layer probe, is given in reference 5. Each shadowgraph was considered as a separate observation, and the transition points on the windward and sheltered sides were noted along with the angle of attack.

Angle of attack.- On the first rounds fired, the angle of attack was found by measuring the angular position of the body axis with respect to fixed reference scales in each station (fig. 3(d)) and by measuring the trajectory of the model center of gravity. Proper combination of these data gave the angle of attack with respect to the

relative wind direction. Later it was found possible to calibrate the angular position of the body axis relative to the shock-wave axis to give the desired information directly at a considerable saving in time. The probable error of this latter method was computed to be 0.1°. The angle-of-attack history, as projected onto the horizontal and vertical planes of the shadowgraph stations, was plotted so that the resultant angle of attack in space could be computed for each shadowgraph. All mention of angle of attack in this report refers to the resultant angle of attack.

Surface roughness.- Surface imperfections were studied and recorded using a metallurgical microscope and an optical comparator at magnifications up to X400. Where possible, profile views of the roughness were photographed. Otherwise, surface views were obtained. Since complete recording of all the model surface was prohibitive, the models were first examined carefully to find the usual surface condition and the outstanding defects. Representative pictures in both categories were then taken. Special attention was given to the nose and nose tip, regions which preliminary experimentation suggested might be critical in determining transition.

The use of a stylus-type profilometer to measure surface roughness was rejected when it was learned that the stylus tip produced a groove in the surface 200 microinches wide (fig. 4). From a magnified view of the shape of the stylus tip, it was calculated that the tip had penetrated the surface to a depth of about 10 microinches. There was, therefore, serious doubt that the tip would respond to the minute imperfections present.[1]

No attempt was made to compute rms roughness height since it was felt that such a presentation could be misleading; a given rms roughness could represent either a large number of small projections or a few large ones. It was felt that the two might have very different effects on the laminar boundary layer.

---

[1]To check the possibility that the profilometer was not functioning correctly, measurements were made of the contact force and the tip diameter. The force of about 1 gram and tip diameter of 1000 microinches were consistent with the manufacturer's specifications. The contact stress due to 1-gram contact force exerted over a bearing area 200 microinches in diameter (corresponding to the width of the groove produced by the stylus) is 70,000 psi, which is equivalent to the known compressive strength of the material. At lesser penetrations of the tip, there is less bearing area and, consequently, higher bearing stresses will occur. Thus, even the harder engineering materials would probably be permanently grooved, although they would have a smaller width and depth of groove.

Surfaces Tested

Models with three different surface finishes were tested. The methods of surface finishing, the characteristics of the surfaces, and the tip geometry obtained will be described below.

Emery-polished surfaces.- The emery-polished models were initially finish-machined; then the surface was smoothed with successively finer grades of emery polishing paper, care being taken at each step to remove scratches from the previous step. The polishing process was completed with 4/0 emery polishing paper, applied in a direction parallel to the model axis. The resulting surface, which appeared to the eye to be a polished, moderately bright surface, is shown by the photomicrograph (fig. 5(a)) to be densely covered with fine scratches. The depth of the scratches was investigated by polishing a model tip circumferentially with 4/0 paper and photographing the tip contour (fig. 5(c)). The deepest scratches were estimated from this picture to be 50 microinches in depth.

Screw-thread surfaces.- Exceedingly fine screw threads were machined on the surface of a second group of models, resulting in a continuous series of two-dimensional grooves normal to the air flow. Models were made with threads of different depths in the range from 0.0001 inch to 0.0010 inch. The grooves on any given model were of uniform depth. The grooves were machined with a tool having a nose angle of $136^\circ \pm 0.5^\circ$, the cutting tip of which was kept as sharp as practically possible. However, the finest threads cut were mostly within the region of curvature of the tool tip and when viewed in profile are best described as a wavy surface (fig. 6(a)). The coarser threads have the geometry of a longer section of the tool tip and show straight sides and 136° included angle (fig. 6(b)). Machining of the threads all the way to the model tip was attempted but, in the process, the tips were bent. It was necessary, therefore, to straighten them by stoning while the model was turning in the lathe. The tips produced were not smooth when viewed at X400 (see fig. 6(c)), but were covered with annular scratches up to 0.0002 inch deep.

Diamond-polished surfaces.- A third group of models was polished initially using the emery polishing procedure described above; then metallurgical polishes of successively finer size were applied. The final polish consisted of a diamond compound with particles averaging 10 microinches in size. Representative photomicrographs of the surface produced are shown in figure 7. These pictures indicate that almost all scratches visible with 400 power magnification have been removed. The dark spots on the surface are inclusions that failed to go into solution during the heat treatment of the 75 ST. The number of inclusions was estimated to be about 1 million per square inch of surface or about 3 million per model. Since the inclusions were harder

than the matrix, the polishing processes tended to wear away the matrix faster than the inclusions. The diamond compound was of sufficient hardness to cut the inclusions at nearly the same rate as the matrix. At best, however, the final surface was inferior to one which could have been produced if the inclusions had not been present.

Since seven shadowgraph pictures were, in general, insufficient to define the experimental curves, it was necessary to launch a number of physically identical models. The information contained in this report was obtained from 36 models. As an aid in classifying the tests performed, the disposition of these models is given below:

Type of surface	Thread height, in.	Number of models tested	
		R_l = 12 million	R_l = 24 million
Emery-polished	- - -	12	2
Screw-thread	0.0001	0	1
	.0002	2	7
	.0003	2	0
	.0004	0	1
	.0005	1	0
	.0007	1	0
	.0010	2	0
Diamond-polished	- - -	1	4
Totals		21	15

In each of the aforementioned classes of model surfaces, certain deviations were made, for purposes which will be discussed later, in either the finish or the tip geometry. In particular, four of the emery-polished models were wax-coated or their tips were bent; the tip profiles of five of the screw-thread models were made to have an abrupt change in slope a few hundredths of an inch from the tip; and two of the diamond-polished models were polished to a greater degree of smoothness than the other three.

EXPERIMENTAL RESULTS

Some of the experimental results to be presented here are concerned with the stated purposes of this investigation; others were accepted as necessary consequences of the method of testing (angle of attack) or were happened onto accidentally in the course of the work. For this reason they do not form a single, unified picture. These results will be presented in this section and briefly interpreted, where possible, in the Discussion section to follow.

Tests at a Reynolds Number of 12 Million

Emery-polished models.- The first tests attempted were with emery-polished models having the longitudinal scratches described above. The ratio of maximum scratch depth to boundary-layer thickness was 0.03.[2] Successful data were obtained with eight models at angles of attack in the range from 0° to 3.5°. It was evident that the angle of attack and circumferential position (windward or sheltered) were influencing the transition point, so the data were separated into windward and sheltered data and plotted against angle of attack, as shown in figure 8. The windward side remained laminar up to the maximum angle of attack (in 28 out of 34 cases) but the sheltered-side transition point moved forward rapidly starting at $\alpha = 1^\circ$. Shadowgraph pictures of two of these models at angles of attack of 1.3° and 2.7° are shown as figures 3(a) and 3(b)

The shadowgraph pictures were not, in general, parallel to the plane of angle of attack. Therefore, the fully windward and fully sheltered sides were seldom seen. The data presented in figure 8 were plotted against meridian angle θ which is, by definition, 0° on the full windward and 180° on the full sheltered side, and the results are given in figure 9. For α less than 1° no variation of R_T with meridian angle could be detected since all the surface was laminar. At the larger values of α, the transition point appears to be nearly constant over each half of the body. The scatter in these figures is moderate considering the fact that angle of attack, while limited to the small ranges given in each figure, is not constant and also that the transition point may, in reality, be varying somewhat with time, a factor which would show on this plot as scatter.

---

[2]Definition of the ratio of scratch depth to laminar boundary-layer thickness, h/δ, is complicated by the fact that the boundary-layer thickness increases along the body, whereas the roughness height on the models in the present test is nominally constant. Thus, h/δ is infinite at the tip for any degree of roughness and is minimum at the body base. Since it is not known which of the possible values of h/δ is most significant or whether any single value of h/δ is significant under these circumstances, the choice of h/δ must be arbitrary. Throughout this report, except where otherwise stated, h/δ was evaluated at the station where Reynolds number was 1 million. The laminar boundary-layer thickness was calculated using the momentum integral method for bodies of revolution (see, e.g., ref. 6). The velocity and density profiles were assumed to be those of a flat plate at the local body Mach number (taken from ref. 7). The boundary-layer thickness δ was defined as the distance from the surface at which the local velocity attained 0.995 of the inviscid-flow velocity.

Screw-thread models.- Two models with thread heights of 0.0002 inch and two with thread heights of 0.0003 inch were tested. The corresponding h/δ values were 0.11 and 0.17. The data are plotted in figure 10 and are very similar to those in figure 8. The effect of meridian angle was examined and found to be very similar to that found with the emery-polished models. Figure 3(c) is a shadowgraph picture of one of these models.

Because the flow was fully laminar over the fine-thread models at small angles of attack, tests were conducted with increasing thread height to define the effect of roughness. Models with thread heights up to 0.0010 inch ($h/\delta = 0.56$) were prepared and tested. Shadowgraph pictures obtained with two of these models are shown in figures 3(d) and 3(e). Data for three of the models are plotted against angle of attack in figure 11. Transition occurred ahead of the positions indicated by the sheltered-side curves (figs. 8(b) and 10(b)), and an apparent consequence was that no strong angle-of-attack effects were observed and there were no systematic differences between the data for windward and sheltered sides. The transition point moved randomly over a range of 2 to 3 million Reynolds number, an effect that would undoubtedly be recognized as a transition region if measurements were made with a pitot tube or other averaging instrument. The skin-friction and heat-transfer characteristics of the transition region depend on the fraction of the time that turbulent flow exists at any body station. The limited number of pictures available was analyzed to determine this fraction by noting the percent of the observations in which a given body station was turbulent. For example, in figure 12, on the curve for $h/\delta = 0.39$, 4 observations out of a total of 14 showed turbulent flow at the body station, $R = 5$ million, so the fraction 4/14, or 29 percent, is, within the limitations of the small sample, the percent time that this station was turbulent. The coarse screw-thread data of figure 11 are given this type of presentation in figure 12. Thus, for $h/\delta = 0.39$, the flow is fully laminar to a Reynolds number of about 4 million, transitional from 4 to 7 million, and fully turbulent beyond 7 million.

The effect of increasing thread height on transition Reynolds number is shown in figure 13(a) where the average of the observed values of transition Reynolds number is plotted against thread height. The transition point moved forward rapidly with increasing roughness. The numerical values shown may be strongly affected by the axial pressure distribution, an effect that has not as yet been systematically explored.

Since transition occurred beyond the limit of observation for both the fine screw thread and the emery-polished surfaces at low angles of attack, it seemed that no new information could be obtained by testing a model having a surface smoother than either of these at a body length Reynolds number of 12 million. Accordingly, tests at a higher length Reynolds number were attempted.

Tests at a Reynolds Number of 24 Million

In an attempt to define the transition curves for Reynolds numbers greater than 11 million, the wind tunnel was pressurized to 2 atmospheres static pressure. It was recognized that increasing the Reynolds number in this way would thin the boundary layer and result in effectively rougher surfaces, but it was felt at first that this effect could be taken into account. The surface finish chosen for study and comparison of the results at the two Reynolds numbers was the screw thread, since this surface offered the greatest possibility for controlled variation of amplitude while maintaining similar roughness form.

Screw-thread models.- Data were obtained at length Reynolds numbers of about 24 million (2 atmospheres pressure) with screw-thread models ranging in thread depth from 0.0001 inch to 0.0004 inch. Transition occurred at far smaller Reynolds numbers than on the corresponding models tested at atmospheric pressure. In plotting the results, the values of h/δ had to be adjusted for the change in boundary-layer thickness caused by the increased static pressure. At a given body station, h/δ varies directly as the $\sqrt{R}$ so that doubling R roughly increases h/δ by 40 percent. At a given Reynolds number station, h/δ varies directly with the Reynolds number per inch so that doubling R_l approximately doubles h/δ.[3] Adjusting the boundary-layer thickness by either of these methods improves the agreement of the data obtained at the two static pressures but even the larger adjustment was insufficient to bring about complete agreement, as is shown in figure 13(b). The remaining disagreement is attributed to the influence of the axial pressure distribution. The theoretical axial pressure distribution on an ogive cylinder, as given in reference 8, is plotted in figure 14 against body-station Reynolds number. The stabilizing effect of favorable pressure gradient on the nose extends, at a static pressure of 1 atmosphere, to a Reynolds number of 2 million but, at 2 atmospheres, extends to a Reynolds number of 4 million. The increased tolerance to roughness shown in the data of figure 13(b) below a Reynolds number of 4 million is probably a reflection of this effect. The destabilizing effect of the adverse pressure gradient behind the nose is applied at higher Reynolds numbers in the tests at 2 atmospheres. This may be the cause of the reduced laminar runs for the fine screw threads at 2 atmospheres static pressure.

Emery-polished models.- Two emery-polished models were tested at a length Reynolds number of 24 million and were found to be covered with bursts of turbulence (fig. 3(f)). Turbulence was observed at Reynolds

[3] Because the flow varies in character from conical at the model tip to cylindrical beyond the nose, the factor is not exactly 2 but is close to 2.

numbers as low as 6 million and laminar flow was observed at Reynolds numbers as high as 22 million. The fractional time that the local flow was turbulent is plotted in figure 15 against body-station Reynolds number. An extensive transition region, many times the length of the laminar flow region, is indicated.

Diamond-polished models.- Four diamond-polished models were tested at this pressure. The first two had discernible projections on the nose, and large numbers of turbulent bursts were observed. The largest projection found was 75 microinches high and within 0.006 of an inch of the tip, making h/δ, here calculated on a local basis, about 3.0. On the remaining models, a particular effort was made to remove the hard projections by polishing. With these, the number of bursts was greatly reduced.

As was the case with the coarse-thread surfaces at a length Reynolds number of 12 million, no angle-of-attack effect could be discerned. At all angles of attack within the test range, large variations in the instantaneous transition point were observed as is shown in figures 3(g) and 3(h), which are two pictures of the same model taken 1 millisecond apart. The resultant angle of attack was 0.6° in both cases. The variation in the instantaneous transition point is shown graphically in figure 16 where the fraction of the time that the local flow was turbulent is plotted as a function of the body-station Reynolds number. The data from the individual models did not coincide and are therefore plotted separately. It is to be emphasized that these models differed primarily in the number, height, and location of the microscopic three-dimensional projections.

Bursts of Turbulence

In several parts of the investigation, turbulence was observed to occur in limited bursts which would sweep down the body, often followed by laminar flow. The bursts could be identified in the shadowgraph pictures (see, e.g., figs. 3(f) and 3(h)) from their abnormal thicknesses and from the weak shock waves consequently attached to their leading edges. From measurements of the shock-wave angles, the velocity of the bursts on the surface was estimated to be 2400 feet per second or about 60 percent of the free-stream velocity. Interestingly enough, all of the Mach waves emanating from the boundary-layer edge appeared to have nearly the same slope as the burst waves.

Since seemingly identical models often produced decidedly different numbers of bursts, it was evident that the bursts were being caused by subtle factors. Careful attention was given to the study of these factors and the results are summarized below. The number of bursts was measured by the number of shock waves attributable to them. This proved to be a

more sensitive procedure than counting the bursts, which were difficult to detect in the thin boundary layer near the model tip.

Model description	Average number of burst waves per shadowgraph	
	R_l = 12 million	R_l = 24 million
Screw-thread surfaces having low transition Reynolds numbers, h = 0.0005 in. and 0.0010 in.	0	- - -
Diamond-polished surface with projections polished down in vicinity of nose	- - -	1.4
Emery-polished surfaces	.3	8.2
Screw-thread surfaces, h = 0.0002 in. and 0.0003 in.	.3	11.5
Diamond-polished surfaces with minute three-dimensional projections	2.9	10.0
Wax-coated emery-polished surface	3.7	- - -
Emery-polished surface with hooked tip (fig. 17)	5.6	- - -
Hooked tip and wax coating	7.8	- - -
Abrupt change in slope on tip profile, screw-thread surface, h = 0.0002 in.	- - -	26.0

From these data, it appears that the bursts were produced by surface roughness, especially near the tip, and by an abrupt change in slope near the tip, the latter perhaps causing flow separation and eddy discharge. The influence of wax on the model surface was presumed to be one of roughness, since microscopic observation of the waxed surface showed that the wax formed in bumps separated by smooth regions. Greater susceptibility to bursts is indicated in the high Reynolds number tests.

DISCUSSION

Surface Roughness

In the tests at a length Reynolds number of 12 million, two of the surfaces tested, the emery-polished and fine-threaded surfaces, were smooth enough to allow fully laminar flow over the test body at angles of attack less than 1°. It will be shown in the next section that the sheltered-side transition which occurred on these models at larger angles of attack was caused by pressure gradient. Therefore, transition due to roughness did not occur on these surfaces and the two may be regarded as smooth enough for the conditions of the test. The only surfaces on which transition was caused by roughness at a length Reynolds number of 12 million were screw threads of depth greater than 0.0003 inch ($h/\delta = 0.17$), data for which are given on figure 13(a), and those models purposely altered near the tip to produce bursts.

Roughness effects were more pronounced in the tests at a length Reynolds number of 24 million, at which condition transition occurred on the body for every surface tested, even at small angles of attack. The surface that permitted the longest laminar run was one of the diamond-polished models for which transition began at a Reynolds number of 11 million and was incomplete at a Reynolds number of 21 million. The diamond-polished surfaces varied appreciably in their performance depending on the success in polishing down the bumps. The worst one caused earlier transition than the emery-polished surface. The 0.0002-inch screw-thread surface had less extensive laminar flow than the polished surfaces, but a 0.0001-inch screw thread having h/δ of 0.1 was again competitive with the polished surfaces.

The correct method for scaling these results up to full-scale aircraft has not been established experimentally but it seems reasonable to assume that h/δ must be held constant. Also, it appears important to avoid large variations in the pressure distribution as a function of body-station Reynolds number if the present roughness results are to apply precisely. If the present model were scaled up to a length of 50 feet and flown at the test conditions of Mach number and Reynolds number (required altitude - 100,000 feet), the laminar boundary-layer thickness would be increased in direct proportion to the length according to the equation

$$\delta \simeq \frac{x}{\sqrt{R}}$$

Therefore, to keep h/δ constant, roughness amplitude must also be varied in direct proportion to length. Thus, the 0.0003-inch screw thread becomes a 0.03-inch screw thread, and a 50-microinch scratch becomes a 0.005-inch scratch, etc.. Thus, it appears that the present

tests do not represent impractically smooth full-scale bodies. In fact, it is not inconceivable that smoother surfaces than those tested could be produced at full scale with only a moderate effort.

Finally, it should be mentioned that the Reynolds number limitations of the test facility led naturally to the question, "What surface smoothness is necessary to allow laminar flow to a Reynolds number of 11 million, or 22 million?" In cases where the objective is laminar flow to higher Reynolds numbers, with otherwise similar test conditions, smoother surfaces than those indicated here are probably required.

Effect of Angle of Attack

The likeness of the sheltered-side transition curves (figs. 8(b) and 10(b)) obtained at a length Reynolds number of 12 million with two entirely dissimilar surfaces, emery-polished and fine screw-thread, suggests that some factor common to the two sets of data (not surface roughness) is responsible. The rising pressure field on the sheltered side of the body when at angle of attack is one possibility. Two mechanisms by which a rising pressure field can affect transition have been discussed in the literature. One is the effect of pressure gradient on the amplification of small disturbances in the laminar boundary layer. The other is the production of turbulence due to local boundary-layer separation. The former depends on dp/dx; the latter (boundary-layer separation) is usually correlated on the basis of $\Delta p/q_o$. Correlation on the basis of both these parameters was attempted, but no sensible relationship between local pressure gradient and transition point was found. Rather, it appeared that the accumulated effect of pressure gradient as represented by $\Delta p/q_o$ would correlate the data.

First it was assumed that pressure rise along streamlines on the sheltered side of the cylinder was the cause of transition. (The sheltered side of the nose was not considered because it retains a favorable pressure field at the small angles of attack involved.) The first streamline to experience the full pressure rise of the sheltered side of the cylinder is the one that crosses the nose-cylinder juncture at $\theta = 90^\circ$. Attention was therefore fixed on this streamline and it will hereinafter be designated, for brevity, as the critical streamline. The path of the critical streamline on the cylinder can be roughly approximated by the intersection of the cylinder with a plane. The required plane is parallel to the free-stream velocity vector, normal to the plane of angle of attack, and passes through the sides of the cylinder at the nose-cylinder junction. If sheltered-side transition occurs as the critical streamline approaches $\theta = 180^\circ$, then, based on the simple model of the flow given above,

$$\frac{R_T}{R_l} = \frac{x_n}{l} + \frac{1}{2\alpha(l/d)}$$

Or, if transition occurs at some value of θ less than 180°,

$$\frac{R_T}{R_l} = \frac{x_n}{l} + \frac{\sin(\theta - 90°)}{2\alpha(l/d)}$$

In figure 18, these equations are plotted for transition at $\theta = 180°$ and 135° and are compared with the data from figures 8(b) and 10(b). The agreement is surprisingly good. Transition appears to occur near $\theta = 135°$.

The above equation provides a basis for estimating the effects of body geometry on sheltered-side transition, since it contains the geometric variables, x_n/l and l/d. The equation has been applied (assuming transition at $\theta = 135°$) to estimating the angle of attack at which sheltered-side transition first appears on the body for various nose lengths and fineness ratios, and the results are presented in figure 19. Low fineness ratio and large nose to total length ratio are favorable to delaying sheltered-side transition to large angles of attack. Except for the present tests, no experimental verification of these curves is available. They should not be applied when transition is caused by roughness or stream turbulence or any effect other than crossflow pressure rise. At large angles of attack and high crossflow Mach numbers, the pressure distribution around the cylinder may have a different character from that considered here, and furthermore a rising pressure field will occur on the sheltered side of the nose. Figure 19 is not expected to be accurate under these conditions. However, the expectation is that low fineness ratio and long nose sections will continue to be favorable to delaying sheltered-side transition. This remains to be investigated experimentally.

Estimates of the pressure-rise coefficient along streamlines, measured from the point of minimum pressure, were made using slender-body theory (see, e.g., ref. 9). The streamline paths were estimated by the method of Beskin, reference 10, which assumes that the incompressible distribution of crossflow velocity around the cylinder applies and that the axial velocity component is the same as that at $\alpha = 0°$. The computation was made for various streamlines at $\alpha = 3°$ and the results are plotted in figure 20, which shows the variation in pressure rise at a given body station for the sheltered-side streamlines. Transition should first occur on the streamline having the maximum pressure rise. The error due to assuming that transition will first occur on the streamline passing through $\theta = 90°$ at the ogive-cylinder junction can be estimated from this figure. For example, at $x = 2$ inches, the maximum pressure rise has occurred on the streamline which crossed

the nose-cylinder junction at $\theta = 105^{\circ}$. An equal pressure rise will occur on the 90° streamline at $x = 2.1$ inches, so the error in x due to the assumption is 0.1 inch or, in terms of Reynolds number at 1 atmosphere static pressure, 0.2 million. It is apparent that for conditions where the slender-body theory applies, the assumption that the critical pressure rise occurs on the streamline crossing the nose-cylinder junction at $\theta = 90^{\circ}$ is accurate for practical purposes. The inaccuracy due to assuming a plane streamline path to locate the 90° streamline on the body is shown in figure 21.

A principal objective in making the calculations of pressure-rise coefficient was to find quantitative values for the critical-pressure-rise coefficient, measured from the point of minimum pressure to the experimental transition point. Values of the critical-pressure-rise coefficient were calculated for angles of attack of 1°, 2°, and 3° and are plotted against transition Reynolds number in figure 22(a). As Reynolds number is increased, the critical-pressure-rise coefficient decreases. The values obtained are compared in figure 22(b) with subsonic airfoil data (refs. 11 to 16). The subsonic data show a definite trend and are surprisingly consistent considering the fact that they represent data obtained in four facilities (including a free-flight test) on a wide variety of airfoils. The data from the present report unfortunately do not cover the lower range of Reynolds numbers which would make possible a quantitative comparison with the subsonic data. It may be significant that where the Reynolds numbers overlap the magnitudes of critical-pressure-rise coefficient are comparable.

Time Dependence of the Transition Point

Many wind-tunnel experiments have shown the existence of a more or less extensive transition region which appears to be neither truly laminar nor truly turbulent. The measurements which show this are sometimes velocity-profile data, obtained using a pressure probe, or sometimes recovery-factor data, obtained from wall thermocouples, but in any case are obtained with time-averaging instruments. When instruments which are capable of giving instantaneous information are used, such as short-duration shadowgraphs or hot-wire anemometers, the instantaneous transition point appears sharp, but a region which is sometimes laminar and sometimes turbulent with a time-dependent transition point is found. This intermittently laminar and turbulent conception of the transition region has been known for many years but may not have been widely appreciated. Dryden in reference 17 and Jacobs in reference 16 describe, on the basis of hot-wire measurements, the situation exactly as it appears from the present tests.

Pursuing the idea that the instantaneous transition point fluctuates with time, an interesting question is, "By what mechanism does the motion

of the transition point occur?" Two possibilities exist: one, that turbulence begins suddenly in random locations at random times in the form of bursts, as proposed by Emmons and Bryson (ref. 18); second, that the instantaneous transition point wanders smoothly back and forth over the surface. There is no doubt that bursts do exist; they were observed practically throughout the present experiments. They were found to be associated largely with roughness in the vicinity of the tip. It is also true that in some cases, movement of the transition point in the absence of detectable bursts was observed. This does not necessarily refute the hypothesis of Emmons and Bryson since a suitably frequent distribution of bursts in time and position could still be made to represent the experimental observations. Thus, it cannot be proved on the basis of the present tests which of the two processes occur or whether both occur. However, it may be sufficient to state that transition regions were found in which the flow was intermittently laminar and turbulent.

CONCLUDING REMARKS

As a result of these tests with a small-scale slender body of revolution flying through still air at a Mach number of 3.5 with a wall to free-stream temperature ratio of 1.0, certain effects of surface roughness and angle of attack on boundary-layer transition have been observed. Also, some additional observations of the unsteady nature of transition have been made.

Although great care was used in polishing some of the test models of this investigation, the surfaces produced would not be considered particularly smooth at full scale if the test values of h/δ were retained. Nevertheless, fully laminar flow over the test body to a Reynolds number of 11 million was observed on some surfaces at small angles of attack. One particularly surprising result was that fully laminar flow occurred over a model covered with a fine machined screw thread. Relatively fine longitudinal scratches were also found to allow laminar flow. Disappointing results were produced in the case of the models for which the maximum polishing effort was expended. This was attributed to a dense distribution of microscopic three-dimensional projections which the polishing did not remove.

With surfaces smoother than a certain level, the effects of roughness no longer influenced transition and the effects of angle of attack became controlling. In fact, on two very dissimilar surfaces which had fully laminar flow near zero angle of attack, the effect of increasing the angle of attack was essentially the same; that is, the transition point on the sheltered side at a given angle of attack was the same for the two surfaces. This transition was believed due to pressure rise along sheltered-side streamlines and was successfully

studied from this point of view. Equations were derived that agreed with the data and led to the prediction that bodies of low fineness ratios with long nose sections would delay the occurrence of sheltered-side transition to large angles of attack. The critical-pressure-rise coefficients causing sheltered-side transition were found to decrease with increasing Reynolds number.

Transition regions were observed within which the flow was intermittently laminar and turbulent. Unsteadiness of the boundary-layer flow was also evidenced by the occurrence of brief bursts of turbulence which were found to be caused by roughness, particularly near the model tip. For purposes of estimating skin friction and heat transfer, the fractional time that a given body station is turbulent must be known and some of the data are presented in these terms.

In applying these results to other test conditions, the importance of the axial pressure distribution must be recognized. It appeared from the present tests that simply doubling the test Reynolds number by doubling the static pressure so altered the distribution of pressure as a function of body-station Reynolds number as to produce effectively a new test body. Under conditions of uniformly favorable pressure gradient, it would be expected that use of the present roughness data would be conservative.

Finally, it should be noted that although these tests were in the region given by Van Driest for infinite laminar stability to small disturbances, transition due to roughness and adverse pressure gradient still occurred. This is probably not inconsistent with the theory which does not consider disturbances of the magnitude here involved.

Ames Aeronautical Laboratory
National Advisory Committee for Aeronautics
Moffett Field, Calif., Dec. 18, 1953

APPENDIX

ESTIMATION OF MODEL SURFACE TEMPERATURES

In this section the wall temperature of the models of the present test will be estimated. It will be shown that, excluding the extreme tip, the surface temperature will rise only a few degrees Fahrenheit above the initial launching temperature, while the tip itself will rise about 300° Fahrenheit. It is instructive to begin by listing some of the reference temperatures in the problem.

	T	T/T_o
Initial temperature of model	530° R	1.00
Free-stream static temperature	530° R	1.00
Maximum wall temperature for infinite laminar stability (Van Driest)	980° R	1.85
Laminar recovery temperature	1630° R	3.08

Convective Heat Transfer in Flight

The convective heat transfer from the boundary layer to the test model is a complicated problem in which the model temperature varies axially, radially, and with time. Exact solutions were attempted but led to such mathematical complication that they were not pursued, appearing to constitute full research problems in themselves. As a substitute, the problem was divided into parts: the first, to estimate the radial temperature distribution; the second, to determine the axial temperature distribution in the absence of axial heat flow; and the third, to estimate the effect of axial heat flow in the vicinity of the tip.

Radial temperature distribution.- The radial temperature gradient in the model at the surface is determined by the local rate of heat inflow to the model.

$$\left(\frac{\partial T}{\partial y}\right)_{y=r} = \frac{h}{k}\left(T_r - T_w\right)$$

in which $h = 1/2\ C_f\ c_p\ \rho u$. If this slope is assumed to extend to the model center, an order-of-magnitude estimate for the temperature

difference from surface to center is given and is shown in figure 23 as a function of body station for laminar flow. The temperature variations along y (a few degrees Fahrenheit) are negligibly small for present purposes and are hereafter assumed to be zero.

Axial temperature distribution in the absence of axial heat flow.- The time rate of temperature rise due to aerodynamic heating of a short section of cylinder having uniform internal temperature and no heat flow through the ends is given by

$$\frac{dT}{dt} = \frac{2h}{cr\ \rho_m} (T_r - T)$$

which integrates to give

$$T = T_r - (T_r - T_i)\ e^{\left(-\frac{2h}{cr\ \rho_m}\Delta t\right)}$$

This equation was applied to cylinders with appropriate radii and Reynolds numbers to estimate the temperature distribution along the test model in the absence of axial heat flow. The curves obtained are given in figure 24.

Over the entire cylinder and most of the nose, the temperature rise is only a few degrees Fahrenheit. Near the nose tip, temperatures approaching the recovery temperature are computed.

Axial heat flow near the tip.- Axial heat flow, neglected until now, tends to reduce temperatures in the tip below values shown in figure 24. To study this aspect of the problem, consider the conservation of heat energy as applied to the model tip (back to any desired station). The heat which enters the tip from the boundary-layer air is partly stored in the tip and partly conducted through the station chosen as the base of the tip. This can be expressed mathematically as follows:

$$\text{heat entering} = \text{heat conducted} + \text{heat stored}$$

$$\bar{h}\ (T_r - T_w)\ S_w = -\ k\ \frac{\partial T}{\partial x}\ S_b + \frac{1}{3}\ S_b \times \rho_m\ c\ \frac{\partial T}{\partial t}$$

The maximum possible value of the temperature gradient, $\partial T/\partial x$, can be found by neglecting the heat-stored term:

$$\left(\frac{\partial T}{\partial x}\right)_{max} = -\ \frac{\bar{h}}{k}\ \frac{S_w}{S_b}\ (T_r - T_w)$$

This relation gives the maximum possible axial temperature gradient for every body station, and integration of the equation gives the maximum

possible temperature differences between points on the body. To simplify the integration, the wall temperature, T_w, which determines the rate of aerodynamic heating, is conservatively assumed to be constant at its initial value, T_i. The heat-transfer coefficient, $\bar{h}$, is estimated from the Reynolds analogy,

$$\bar{h} = \frac{c_p \rho u}{\sqrt{R/x}} \frac{0.64}{\sqrt{x}}$$

where R/x, the Reynolds number per foot, is a constant. The tip is considered to be conical, so

$$\frac{S_w}{S_b} = \frac{1}{\sin \beta}$$

The final equation for maximum temperature difference between the tip and nose stations near the tip is

$$T_{x=o} - T_x = \frac{1.28 \, c_p \rho u \, (T_r - T_i)}{k \sqrt{R/x} \sin \beta} \sqrt{x}$$

This equation is plotted in figure 25 and shows that the tip point will not be more than 275° hotter than the body station, x = 0.1 inch. For emphasis, it is here repeated that this estimate is conservative in two respects: (1) It gives the temperature differences which are sufficient to conduct out of the tip all of the heat that enters. (2) The aerodynamic heating was allowed to proceed throughout at the maximum initial rate.

Heating Processes in the Gun

During model launching, there are three processes capable of introducing heat into the test model. All of these are transient processes, very difficult to calculate, and, in some cases, fundamental information concerning heat transfer coefficients and the coefficient of friction is lacking. Therefore, only qualitative statements can be made.

Barrel friction.- Although the static friction of the sabot assembly in the barrel is quite low, under the accelerating loads, the parts swell laterally to produce an unknown amount of barrel friction which ultimately is converted to heat at the exterior surface of the lucite sabot fingers. Examination of recovered sabot fingers does not show any evidence of the softening and flowing that would occur in lucite at temperatures above 200° Fahrenheit. If it is assumed that the outside

surface of the fingers is kept at 200° Fahrenheit for 3 milliseconds, the time required for firing and finger separation, the inside surface of the fingers would heat up by only 0.01° Fahrenheit. Therefore, model heating due to barrel friction is negligible.

Heat transfer from the hot powder gases.- Powder gases at temperatures up to 6000° R are in contact for about 2 milliseconds with a nylon sealing plug behind the sabot (see fig. 2(b)). Examination of recovered sealing plugs shows no evidence of melting or flowing at the surface in contact with the powder gas. Therefore, assuming 200° Fahrenheit at the back surface of the plug, the model surface would, in 2 milliseconds, heat only 0.003° Fahrenheit and no heating of the model would result.

Heat transfer to model from compressed air ahead of the projectile in barrel.- This process can best be evaluated by comparison to the forced convection in flight. It occurs for about one-fifth as long as the heat transfer in flight, at comparable temperature potential, but under stagnant (no flow) conditions. It is therefore believed small compared to the heat transfer in flight.

Apparently, the model heating in the gun due to all causes is negligible and the best estimate of model surface temperature distribution is given in figure 25 near the tip and in figure 24 for the remainder of the model. Along 99 percent of the model, the temperature rise is a few degrees Fahrenheit. At the tip, a temperature rise of about 300° Fahrenheit is indicated.

REFERENCES

1. Sternberg, Joseph: A Free Flight Investigation of the Possibility of High Reynolds Number Supersonic Laminar Boundary Layers. BRL Rep. 821, Aberdeen Proving Ground, Aberdeen, Md., June 1952.

2. Czarnecki, K. R., and Sinclair, Archibald R.: An Extension of the Investigation of the Effects of Heat Transfer on Boundary-Layer Transition on a Parabolic Body of Revolution (NACA RM-10) at a Mach Number of 1.61. NACA RM L53B25, 1953.

3. Van Driest, E. R.: Cooling Required to Stabilize the Laminar Boundary Layer on a Flat Plate. Jour. Aero. Sci. (Readers' Forum), vol. 18, no. 10, Oct. 1951, pp. 698-699.

4. Seiff, Alvin, James, Carlton S., Canning, Thomas N., and Boissevain, Alfred G.: The Ames Supersonic Free-Flight Wind Tunnel. NACA RM A52A24, 1952.

5. Jack, John R., and Burgess, Warren C.: Aerodynamics of Slender Bodies at Mach Number of 3.12 and Reynolds Numbers from 2×10^6 to 15×10^6. I - Body of Revolution with Near-Parabolic Forebody and Cylindrical Afterbody. NACA RM E51H13, 1951.

6. Allen, H. Julian, and Nitzberg, Gerald E.: The Effect of Compressibility on the Growth of Laminar Boundary Layer on Low-Drag Wings and Bodies. NACA TN 1255, 1947.

7. Van Driest, E. R.: Investigation of Laminar Boundary Layer in Compressible Fluids Using the Crocco Method. NACA TN 2597, 1952.

8. Rossow, Vernon J.: Applicability of the Hypersonic Similarity Rule to Pressure Distributions Which Include the Effects of Rotation for Bodies of Revolution at Zero Angle of Attack. NACA TN 2399, 1951.

9. Perkins, Edward W., and Kuehn, Donald M.: Comparison of the Experimental and Theoretical Distributions of Lift on a Slender Inclined Body of Revolution at $M = 2$. NACA RM A53E01, 1953.

10. Beskin, Leon: Determination of Upwash Around a Body of Revolution at Supersonic Velocities. Consolidated Vultee Aircraft Corp. DEVF Memo. BB-6, May 1946.

11. Silverstein, Abe, and Becker, John V.: Determination of Boundary-Layer Transition on Three Symmetrical Airfoils in the NACA Full-Scale Wind Tunnel. NACA Rep. 637, 1939.

12. Bullivant, W. Kenneth: Tests of the NACA 0025 and 0035 Airfoils in the Full-Scale Wind Tunnel. NACA Rep. 708, 1941.

13. Schubauer, G. B., and Skramstad, H. K.: Laminar-Boundary-Layer Oscillations and Transition on a Flat Plate. NACA Rep. 909, 1948.

14. Von Doenhoff, Albert E.: Investigation of the Boundary Layer about a Symmetrical Airfoil in a Wind Tunnel of Low Turbulence. NACA WR L-507, 1940.

15. Zalovcik, John A.: Flight Investigation of Boundary-Layer and Profile Drag Characteristics of Smooth Wing Sections of a P-47D Airplane. NACA ACR L5H11a, 1945.

16. Jacobs, Eastman N.: Preliminary Report on Laminar-Flow Airfoils and New Methods Adopted for Airfoil and Boundary-Layer Investigations. NACA WR L-345, 1939.

17. Dryden, H. L.: Aerodynamics of Cooling. Vol. VI of Aerodynamic Theory, div. T, ch. VI, sec. 5, W. F. Durand, ed., Julius Springer (Berlin), 1936, pp. 265-266.

18. Emmons, Howard W., and Bryson, Arthur Earl, Jr.: Transition in a Boundary Layer. Hughes Aircraft Co., Culver City, Calif. Research and Development Labs. Tech. Memo. 245, Sept. 1950.

page 26 is blank

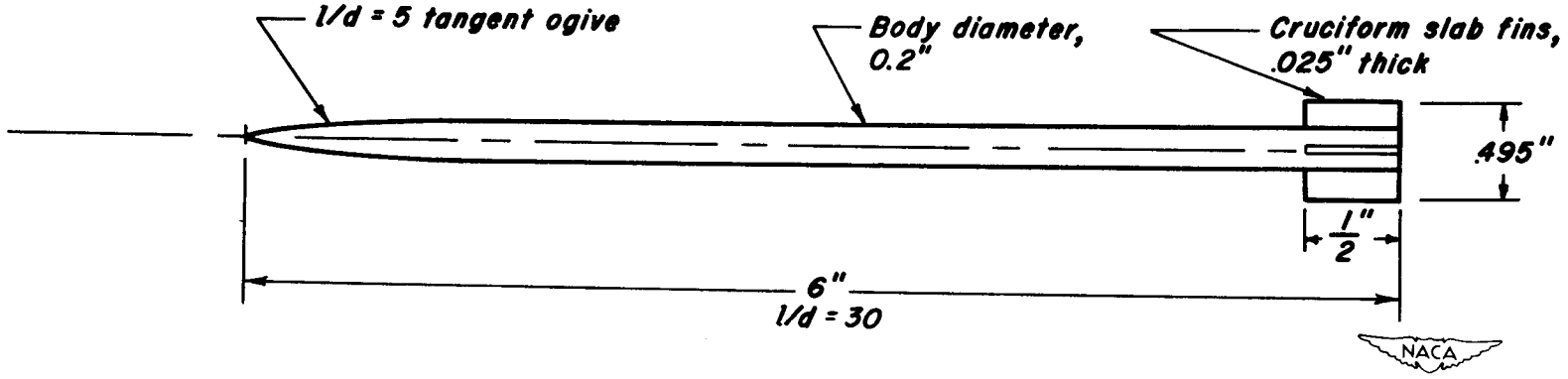

Figure 1.– Typical model dimensions.

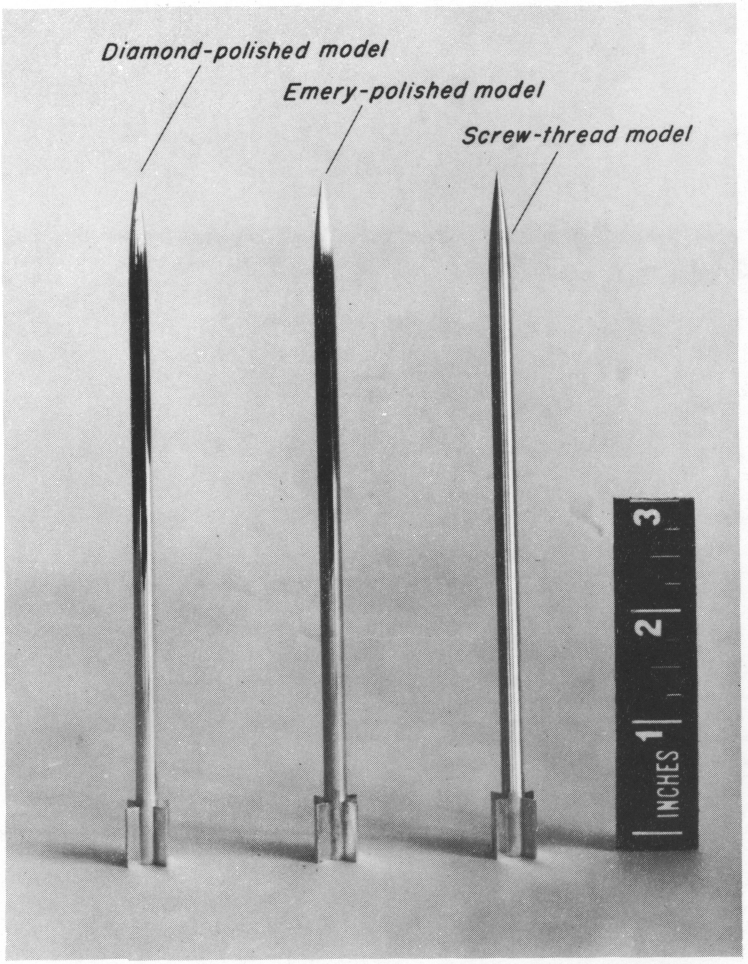

A-18108.1

(a) Typical models.

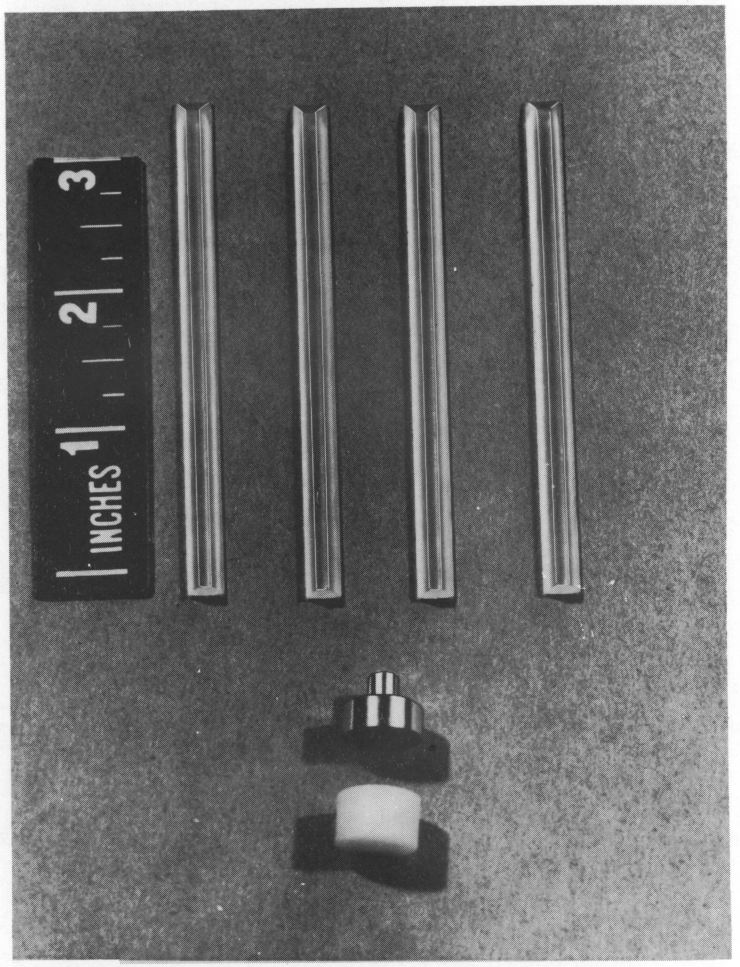

A-18110.1

(b) Sabot parts.

Figure 2.- Models and sabot.

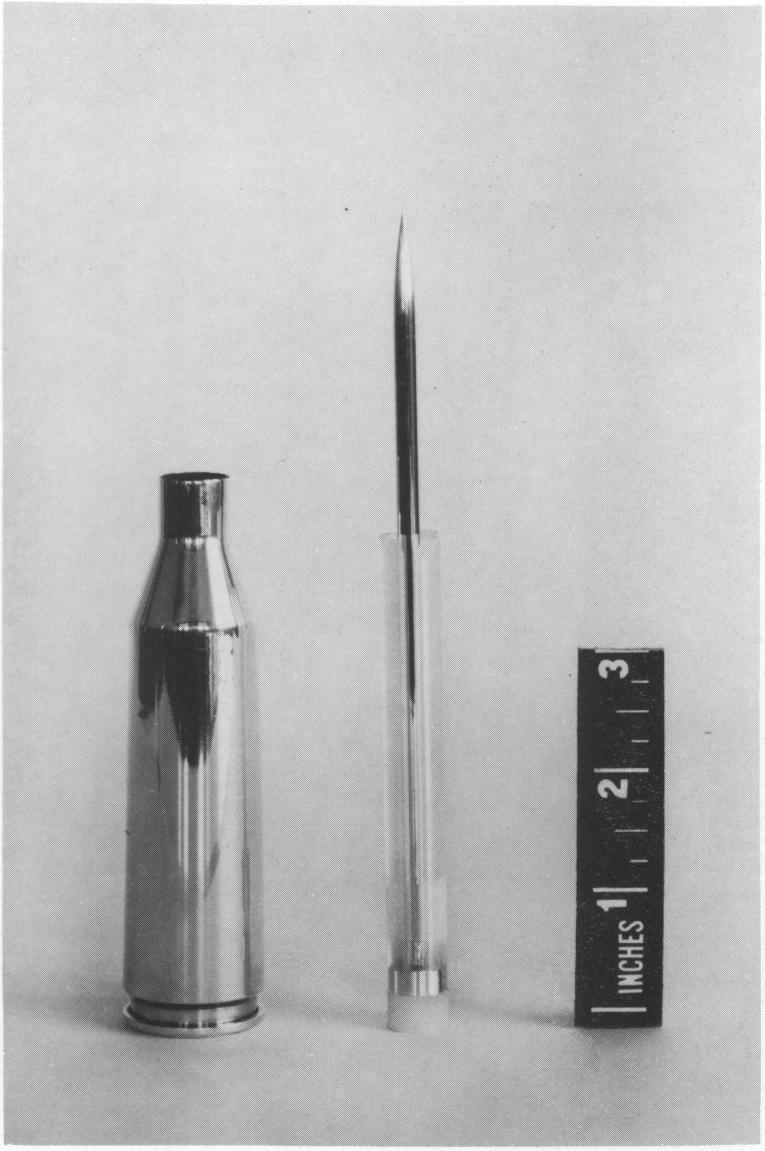

A-18109

(c) Assembly.

Figure 2.- Concluded.

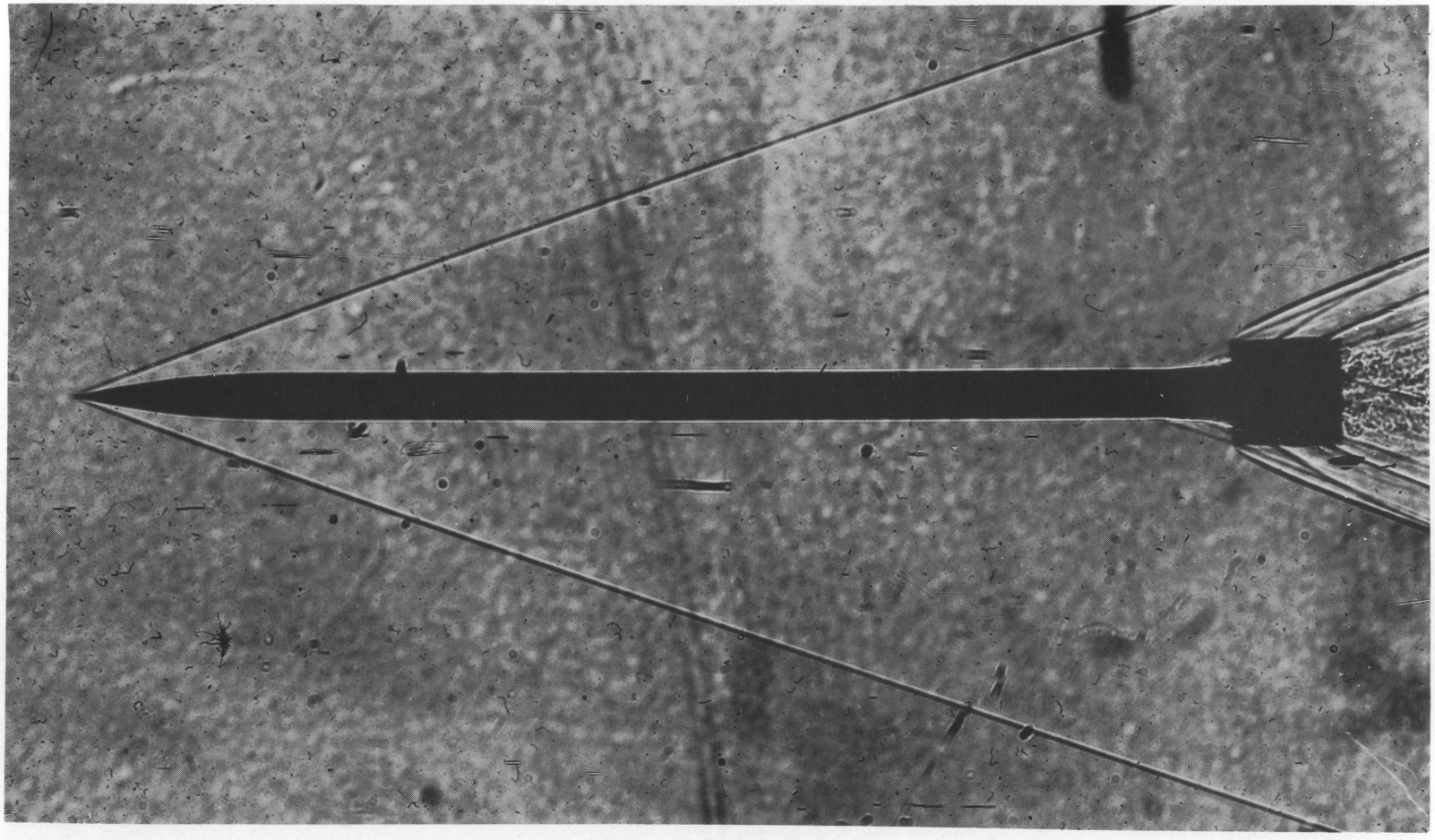

A-18609

(a) Emery-polished model; $\alpha = 1.3^{\circ}$; $\theta = 86^{\circ}$, 94°; $h/\delta = 0.03$; $R_l = 12$ million.

Figure 3.- Shadowgraphs of models in flight.

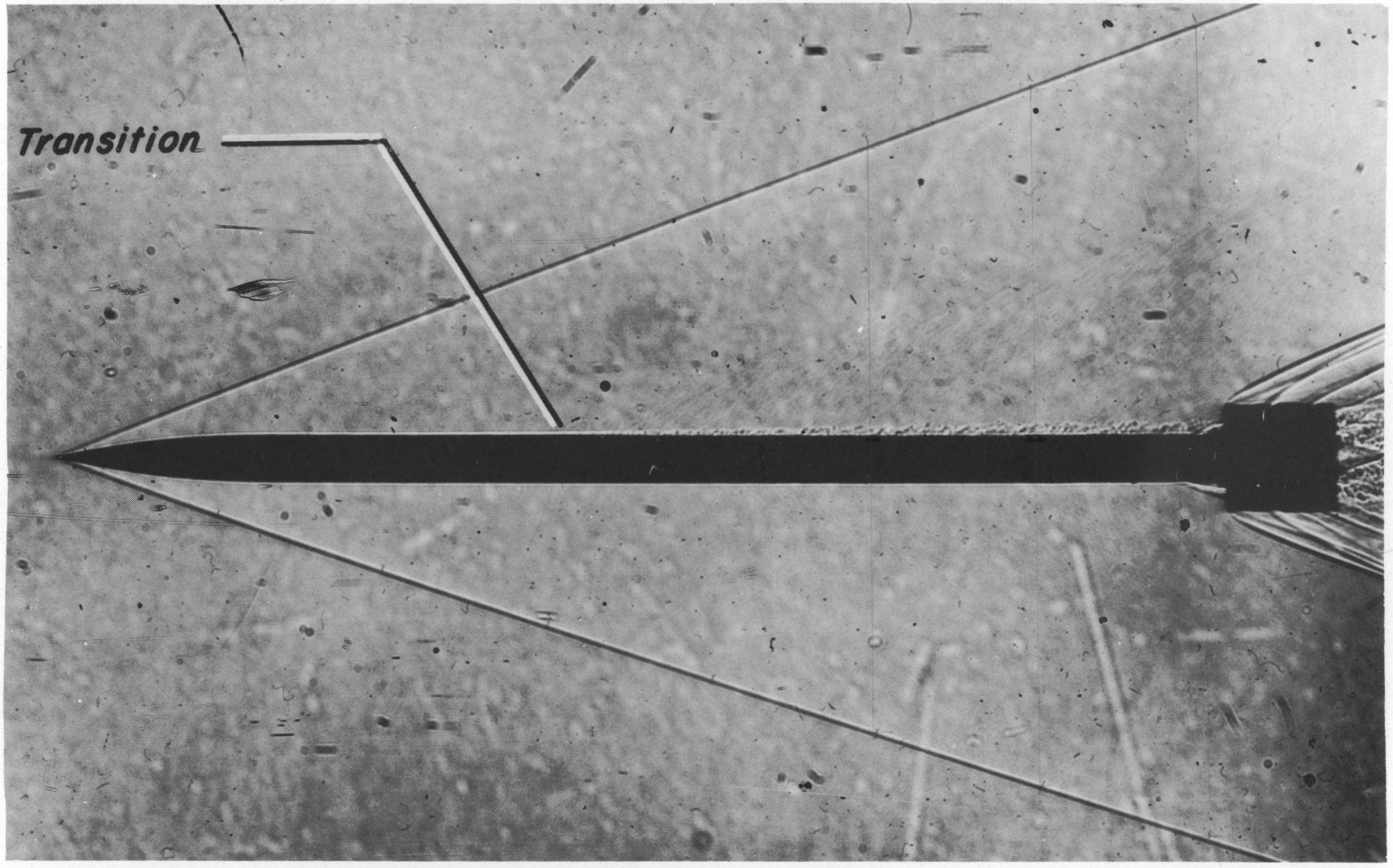

A-18610.1

(b) Emery-polished model; $\alpha = 2.7^{\circ}$; $\theta = 60^{\circ}$, 120°; $h/\delta = 0.03$; $R_l = 12$ million.

Figure 3.- Continued.

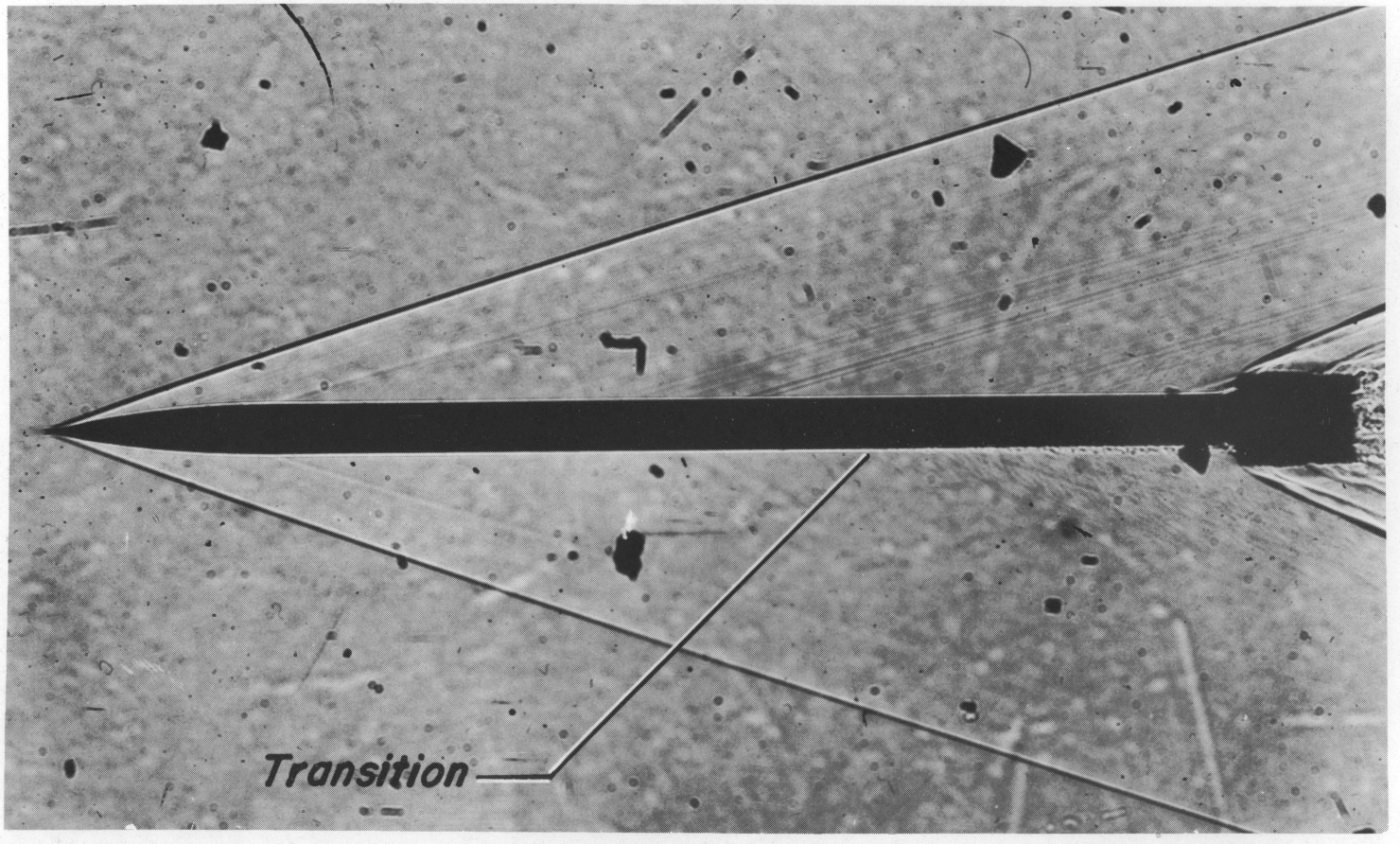

A-18611

(c) Screw-thread model; $\alpha = 1.25^{\circ}$; $\theta = 38^{\circ}$, 142°; $h/\delta = 0.11$; $R_l = 12$ million.

Figure 3.- Continued.

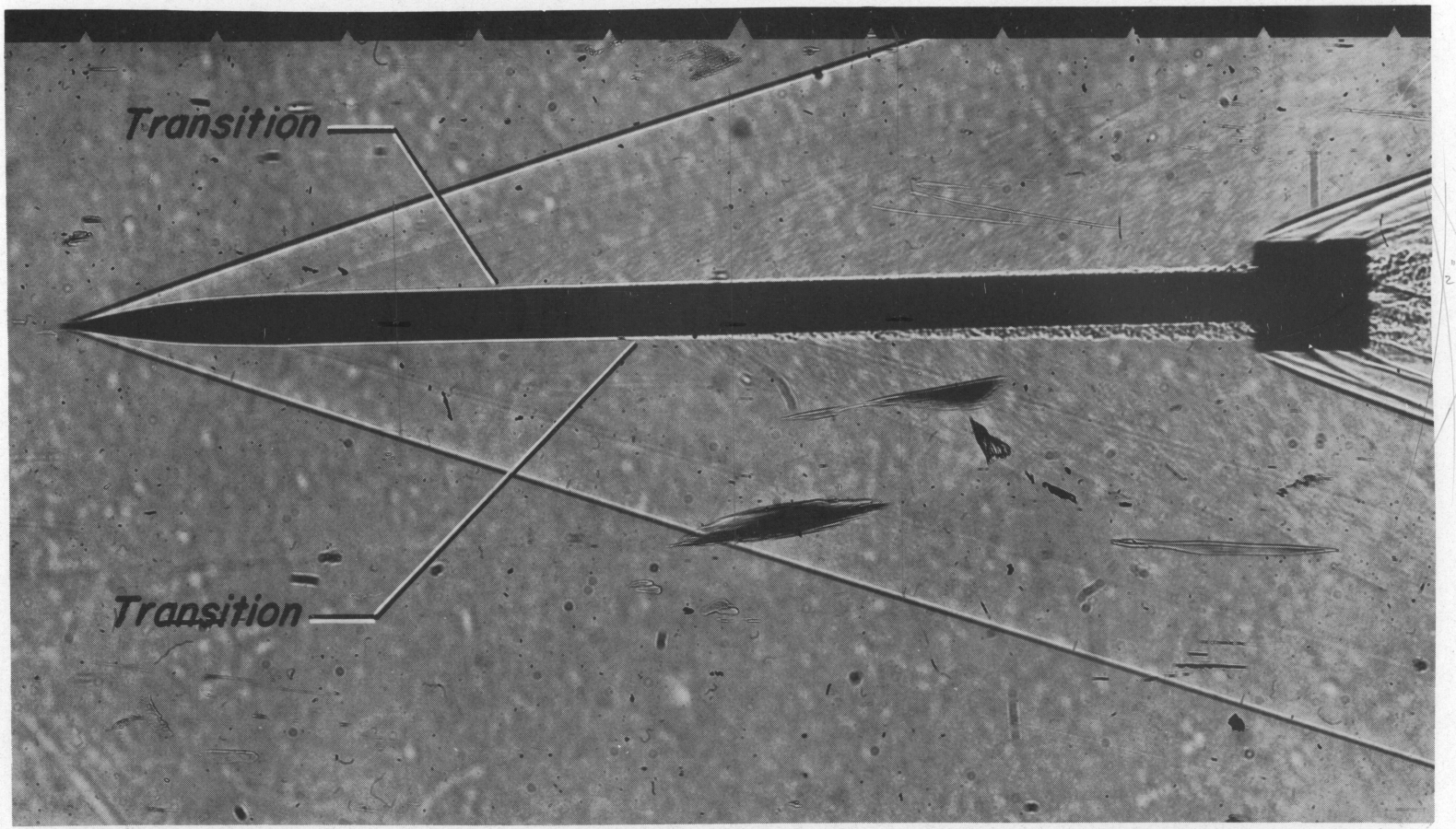

(d) Screw-thread model; $\alpha = 2.2^{\circ}$; $\theta = 56^{\circ}$, 124°; $h/\delta = 0.39$; $R_l = 12$ million.

Figure 3.- Continued.

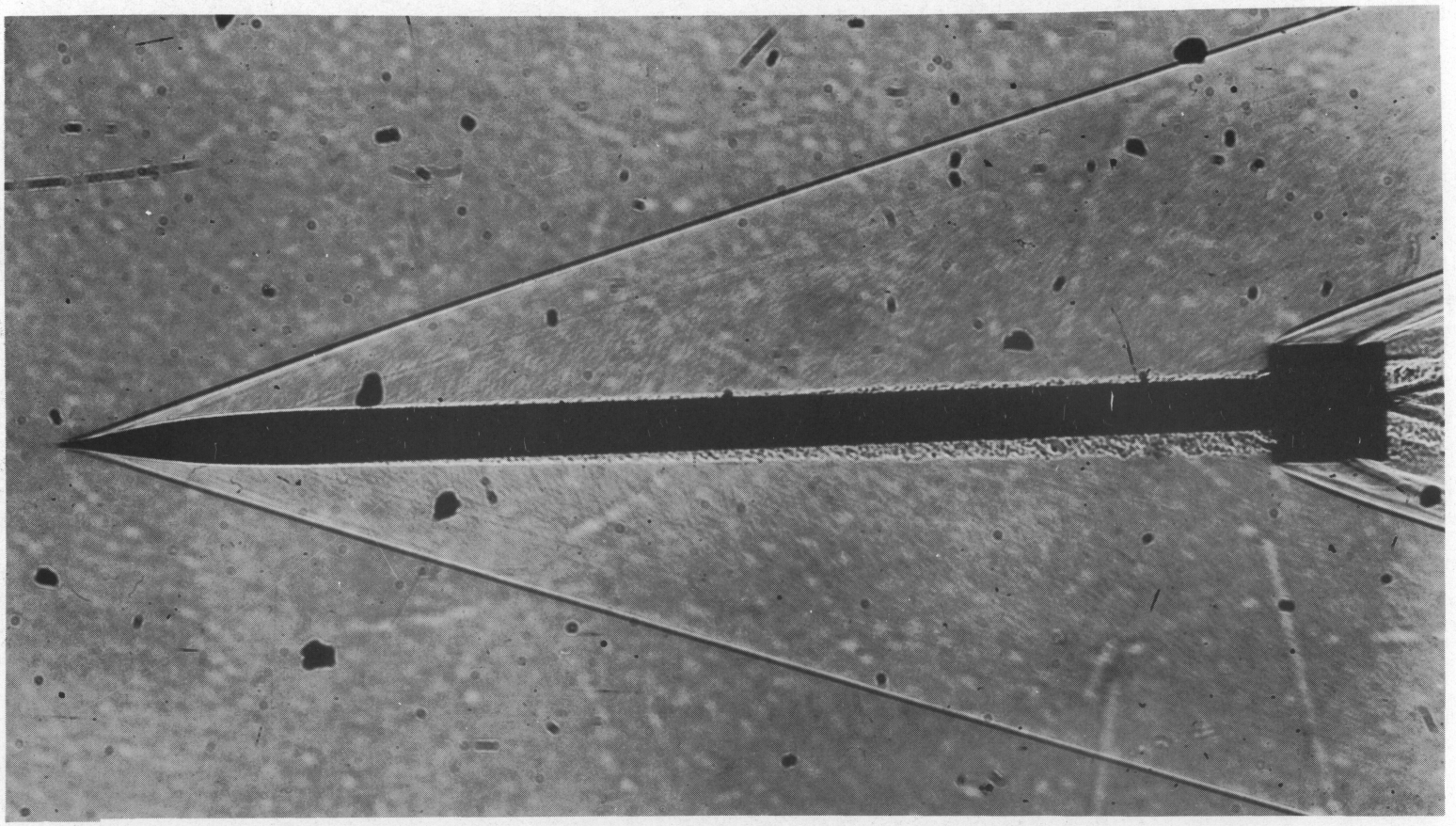

A-18613

(e) Screw-thread model; $\alpha = 1.6^{\circ}$; $\theta = 50^{\circ}$, 130°; $h/\delta = 0.56$; $R_l = 12$ million.

Figure 3.- Continued.

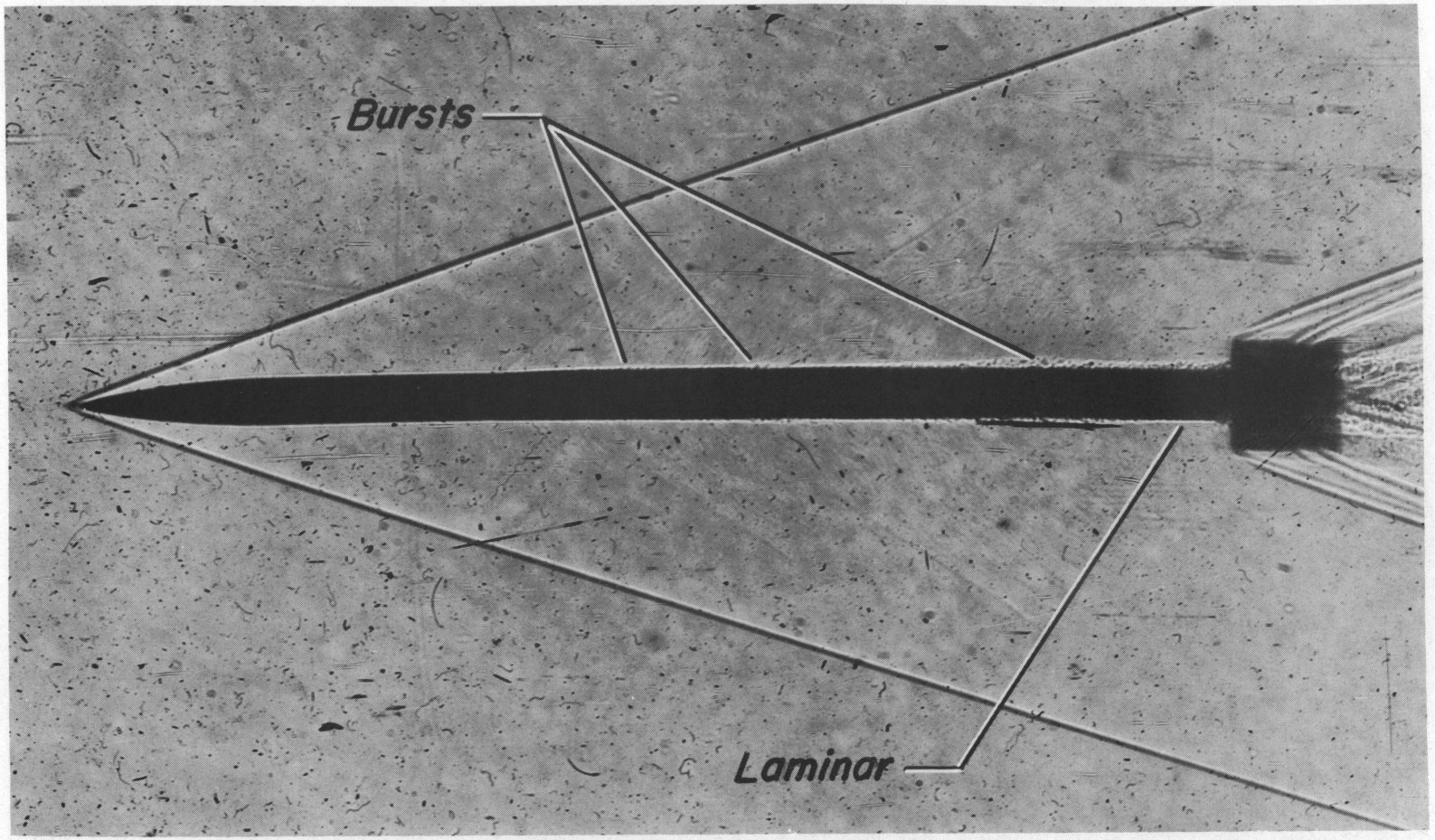

A-18614

(f) Emery-polished model; $\alpha = 0.5^{\circ}$; $\theta = 56^{\circ}$, 124°; $R_l = 24$ million.

Figure 3.- Continued.

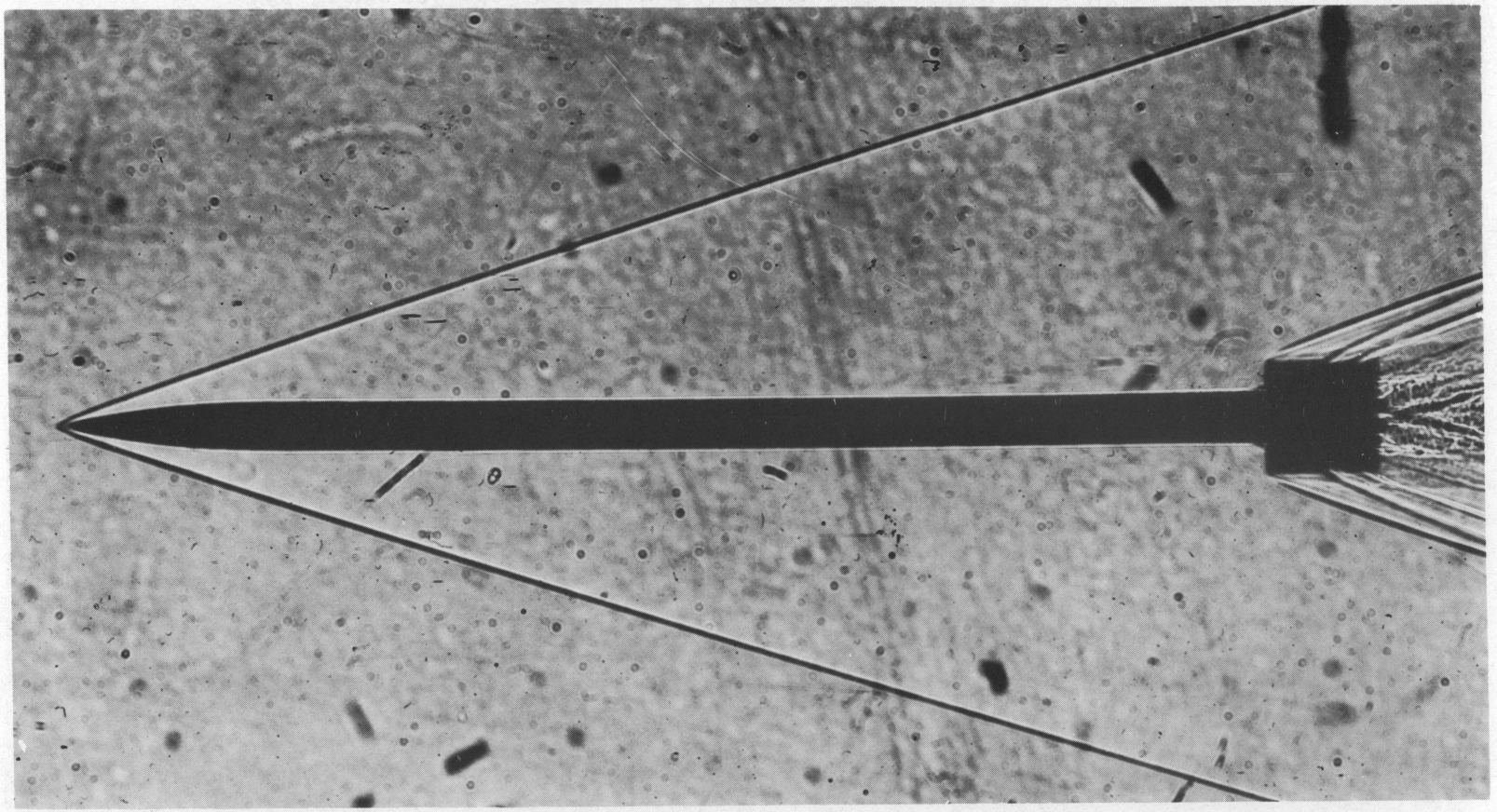

A-18615

(g) Diamond-polished model; $\alpha = 0.6^\circ$; $\theta = 58^\circ$, 122°; $R_l = 24$ million.

Figure 3.- Continued.

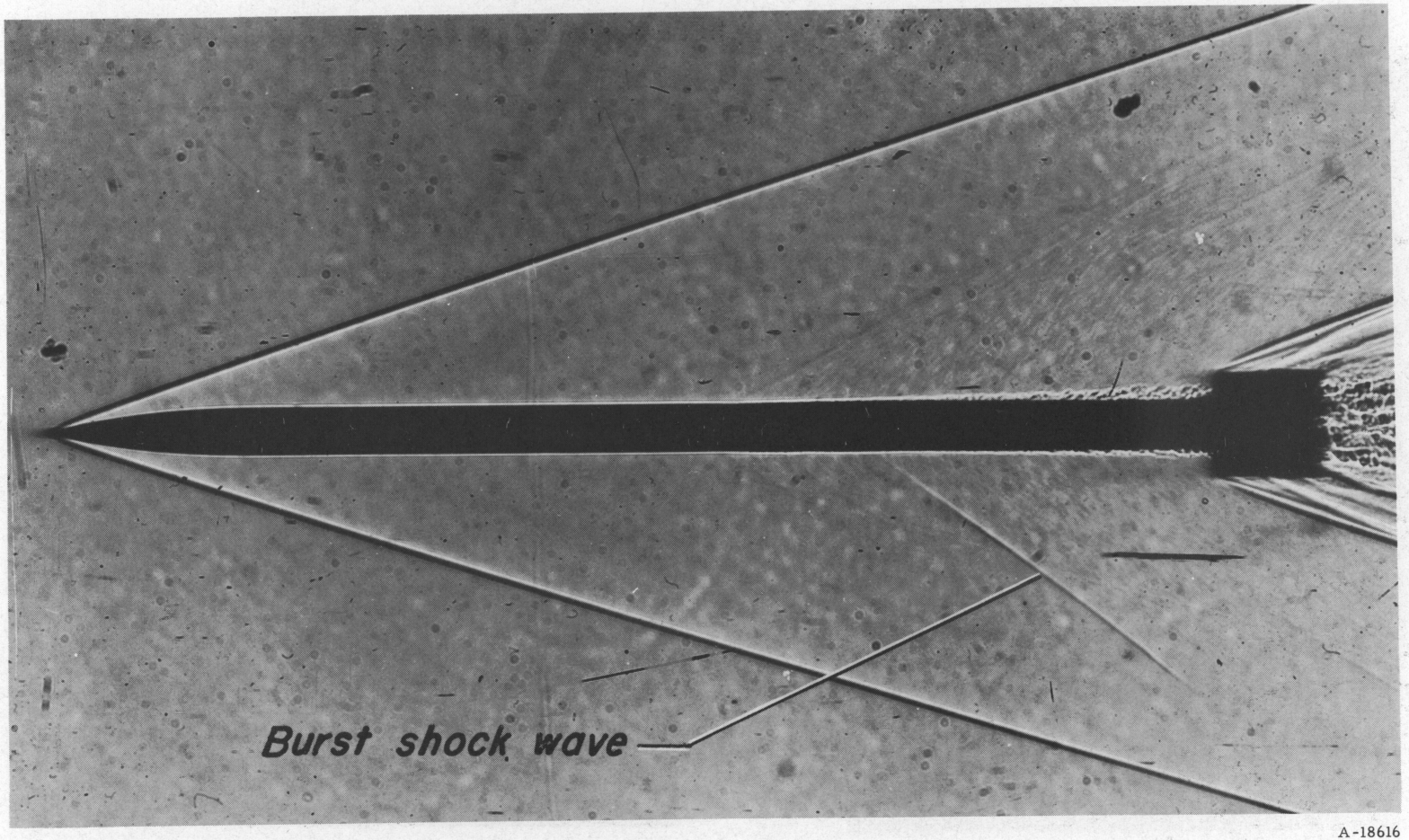

(h) Same model as (g), 1 millisecond later; $\alpha = 0.6^{\circ}$; $\theta = 16^{\circ}$, 154°; $R_l = 24$ million.

Figure 3.- Concluded.

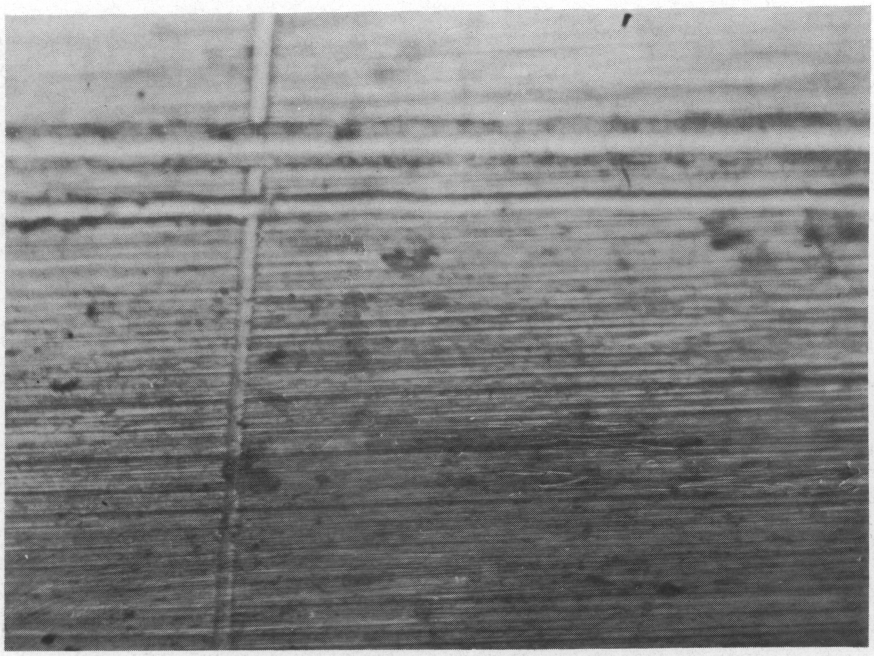

A-18617

Figure 4.- Grooves produced by profilometer stylus on an emery-polished model; X400.

A-18618

(a) Longitudinal scratches on the cylinder; X400.

Figure 5.- Photomicrographs of emery-polished models.

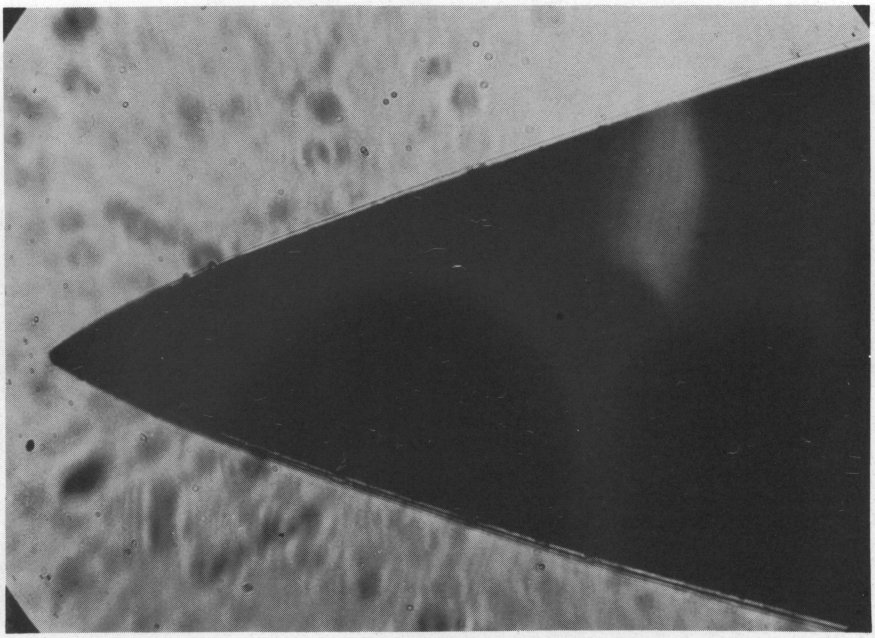

A-18619

(b) Tip profile; X400.

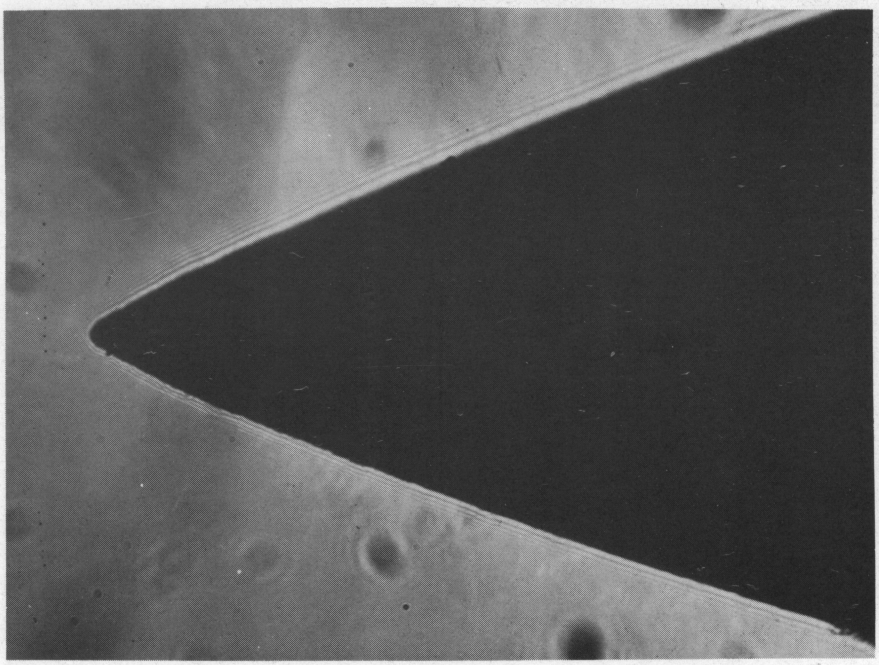

A-18620

(c) Special tip polished circumferentially to allow measurement of scratch depth; X400.

Figure 5.- Concluded.

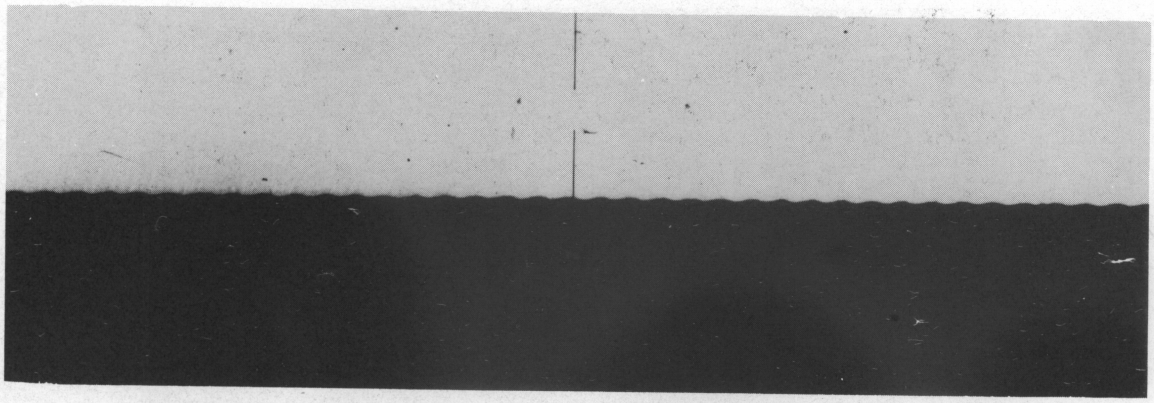

A-18621

(a) Edge profile; h = 0.0003 inch; X100.

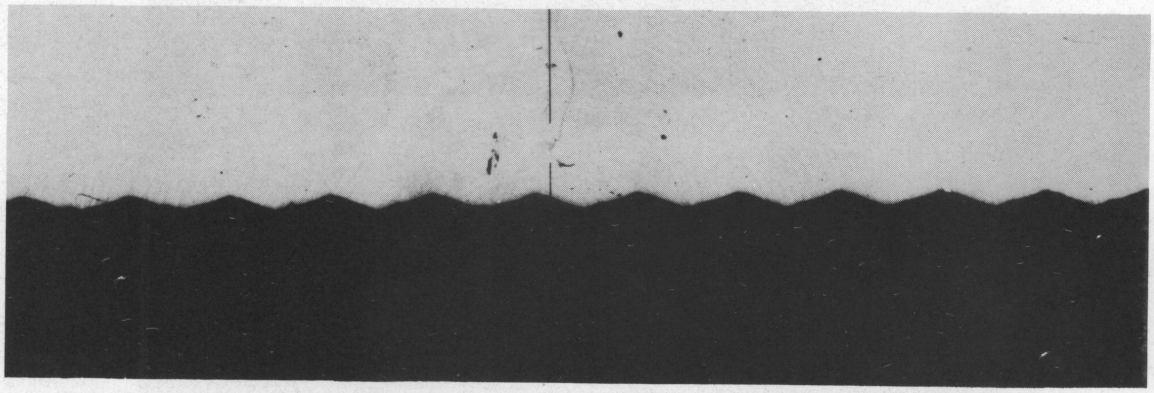

A-18622

(b) Edge profile; h = 0.0010 inch; X100.

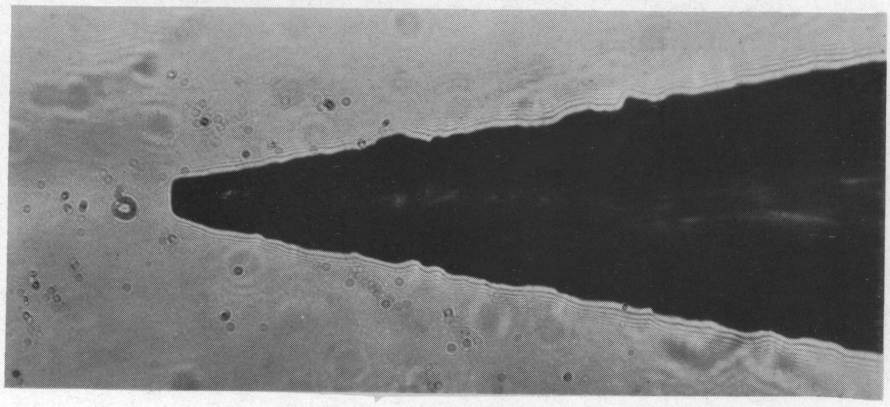

A-18623

(c) Tip profile; X400.

Figure 6.- Photomicrographs of screw-thread models.

A-18624

(a) Representative surface view; X400.

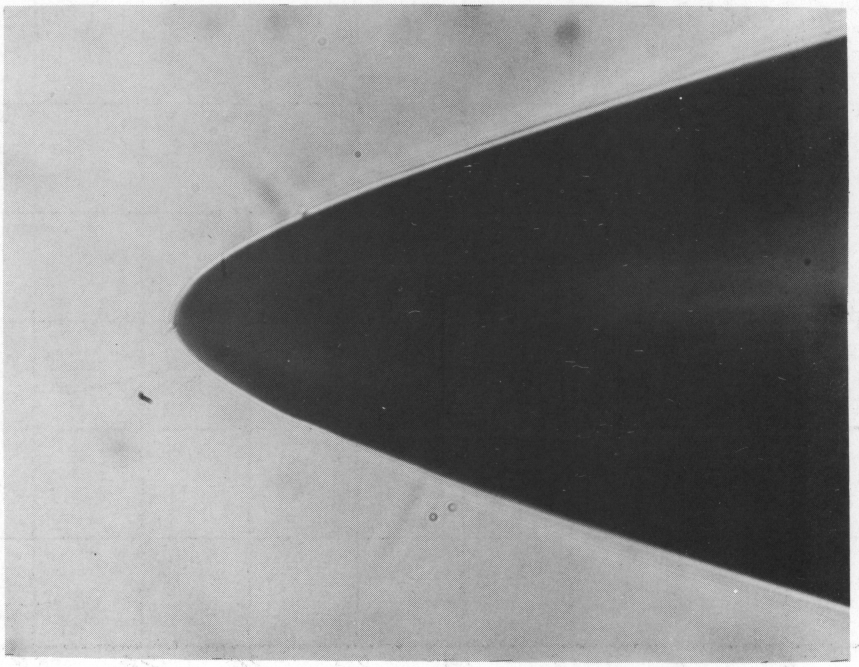

A-18625

(b) Tip profile; X400.

Figure 7.- Photomicrographs of diamond-polished models.

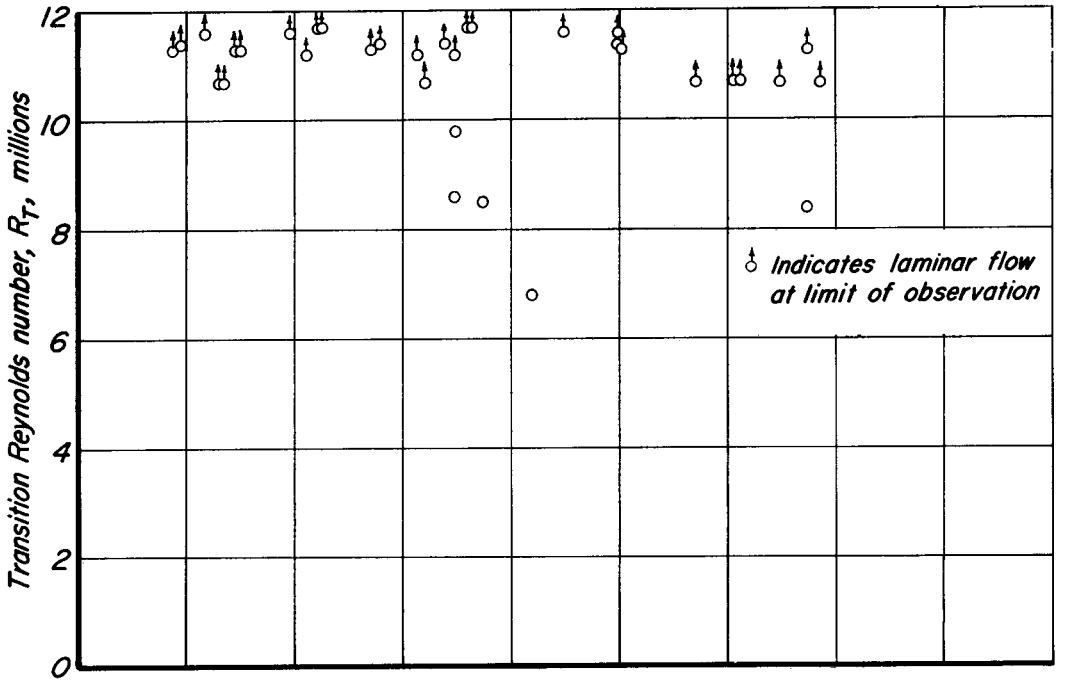

(a) Windward-side observations ($0° \leq \theta < 80°$)

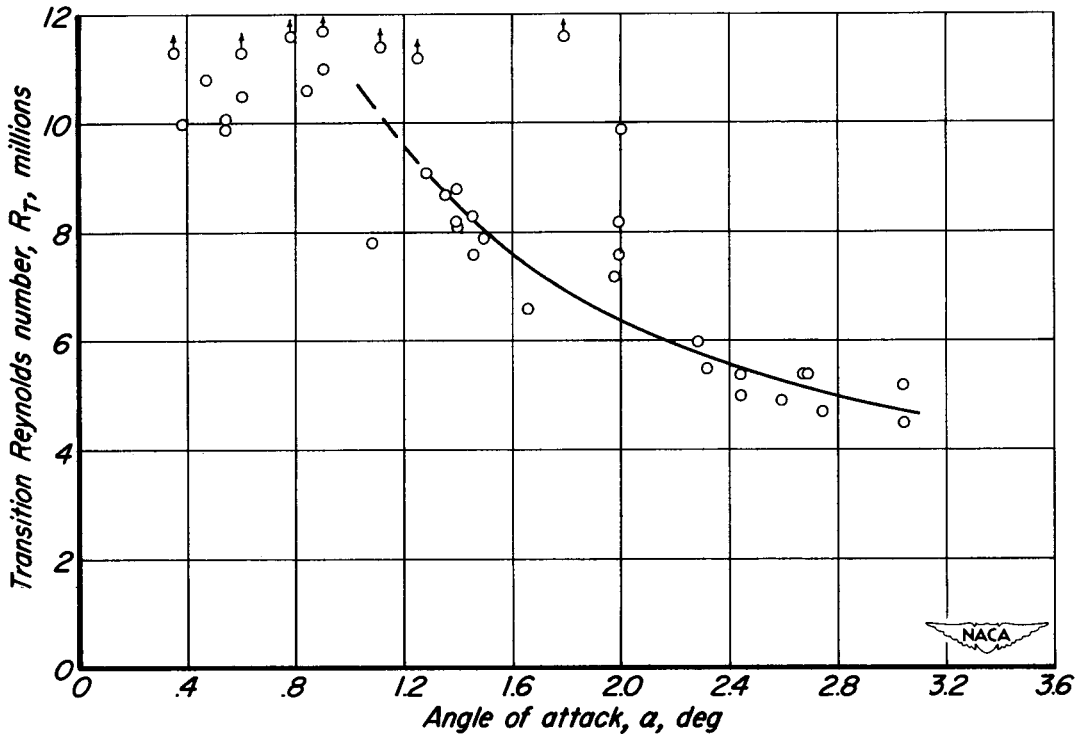

(b) Sheltered-side observations ($100° < \theta \leq 180°$)

Figure 8.- Effect of angle of attack on transition Reynolds number. Emery-polished models; $h/\delta = 0.03$; $R_l = 12$ million.

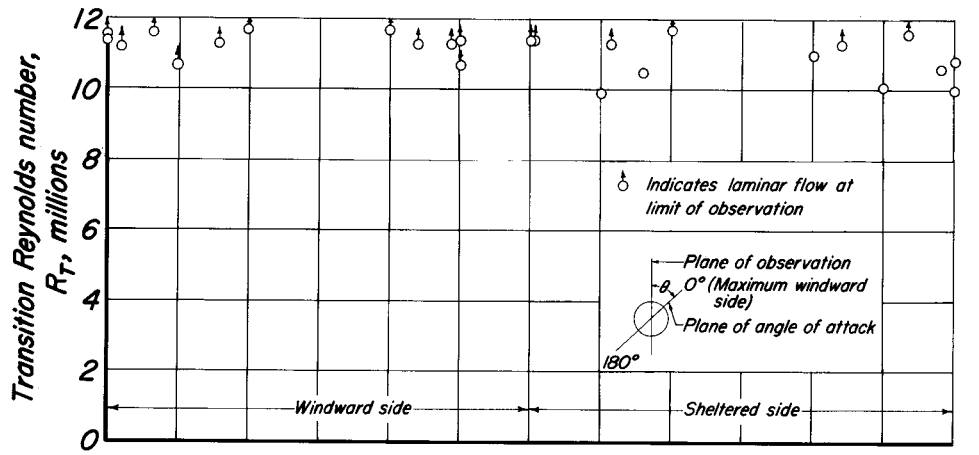

(a) Angles of attack between 0° and 1.0°

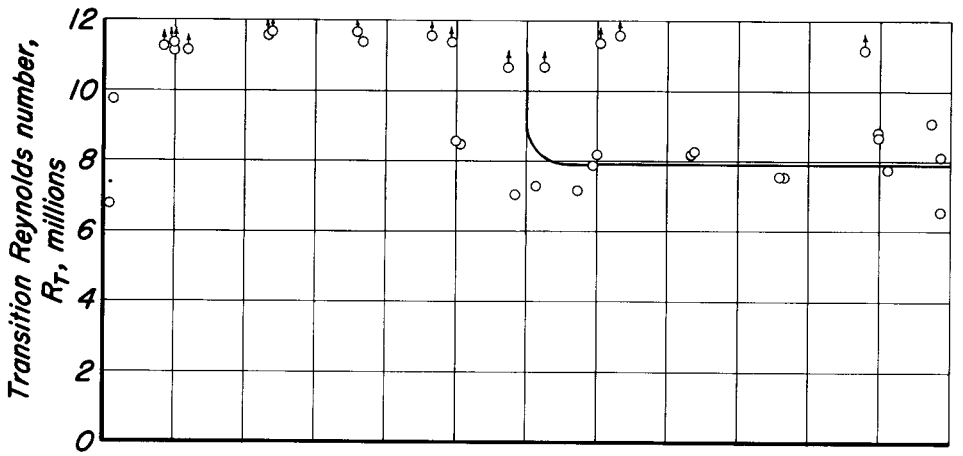

(b) Angles of attack between 1.0° and 2.0°.

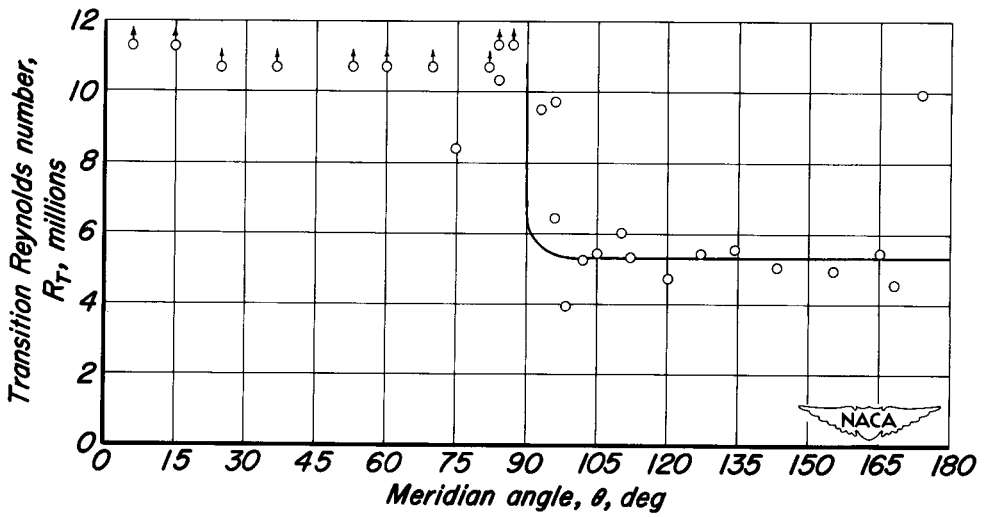

(c) Angles of attack between 2.0° and 3.7°

Figure 9.— Effect of meridian angle on transition Reynolds number. Emery-polished models; $h/\delta = 0.03$; $R_l = 12$ million.

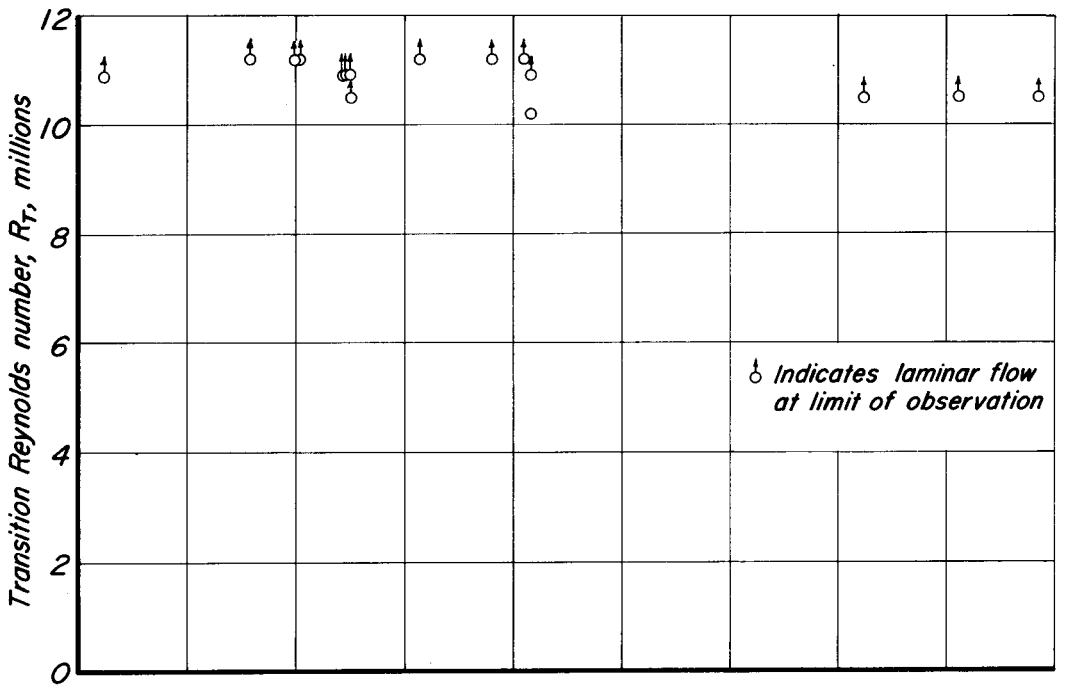

(a) Windward-side observations ($0° \leq \theta < 80°$)

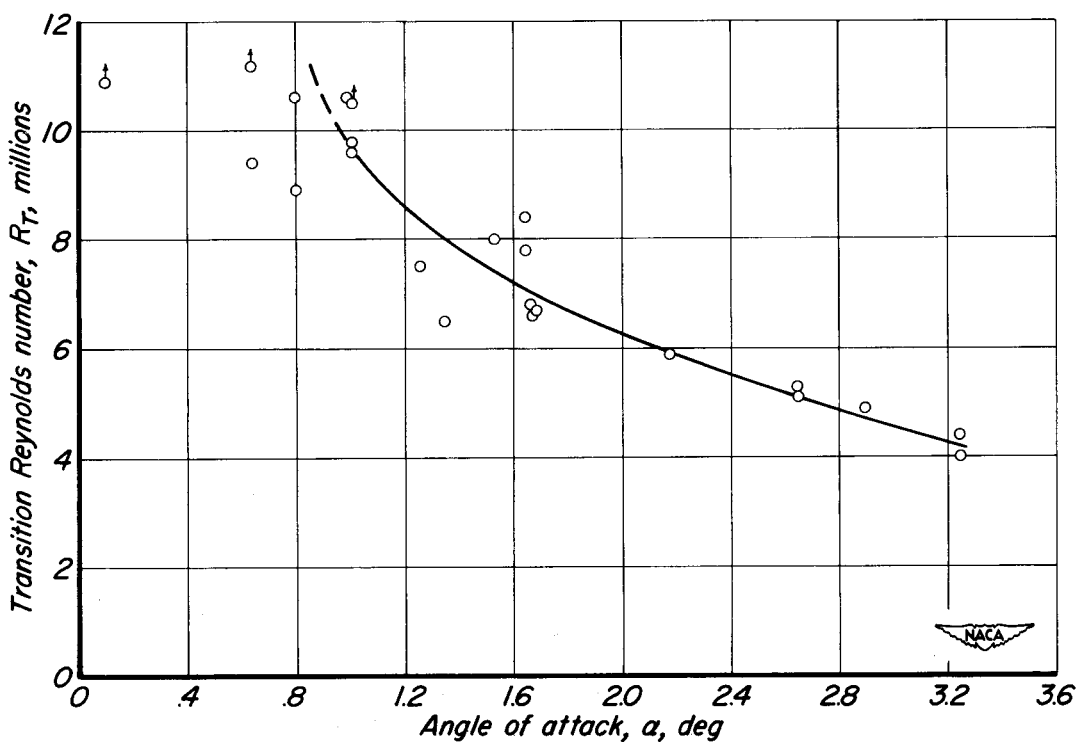

(b) Sheltered-side observations ($100° < \theta \leq 180°$)

Figure 10.— Effect of angle of attack on transition Reynolds number. Screw-thread models; $h/\delta = 0.11$ and 0.17; $R_1 = 12$ million.

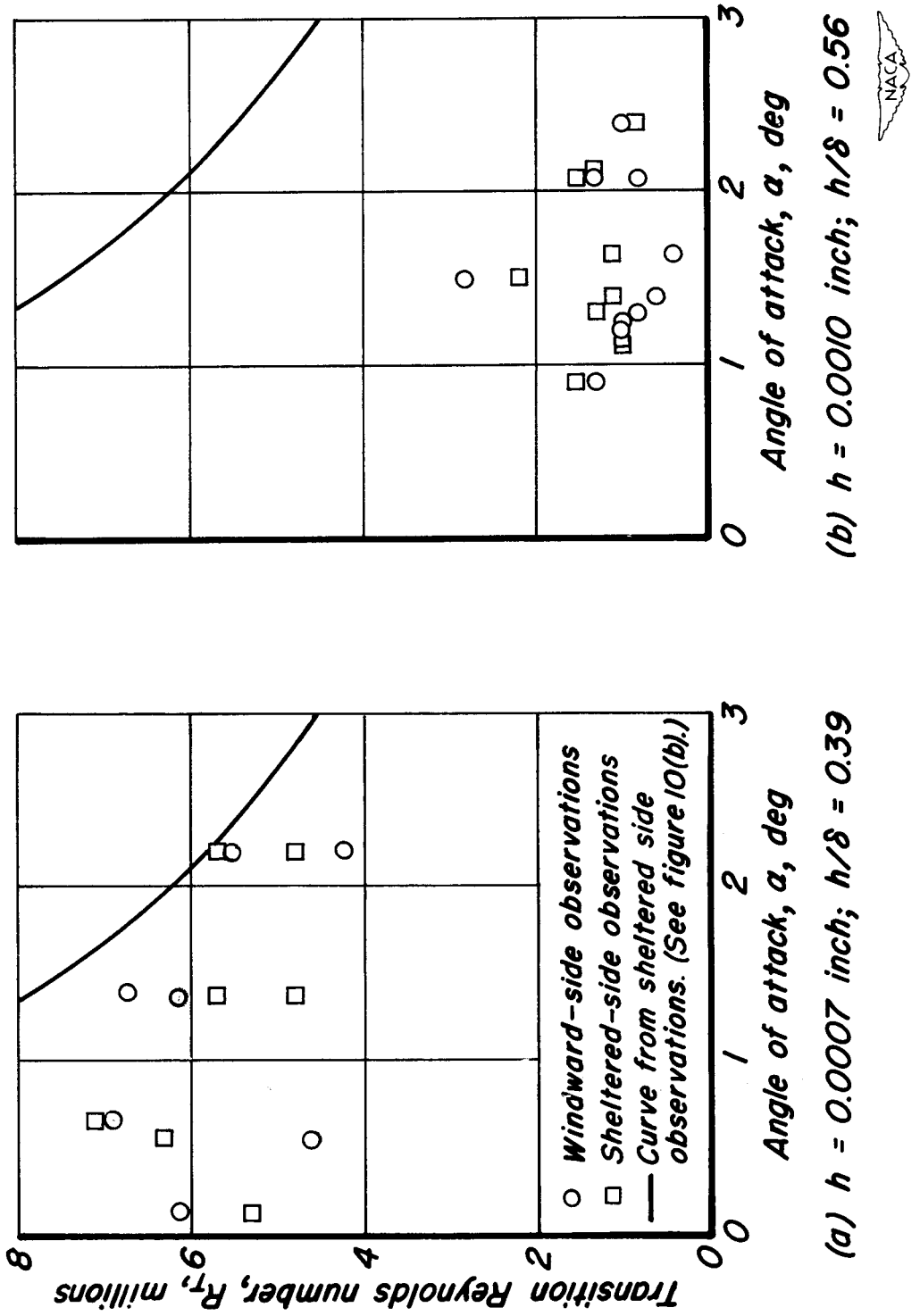

Figure 11.- Data from models with coarser threads; R_l = 12 million.

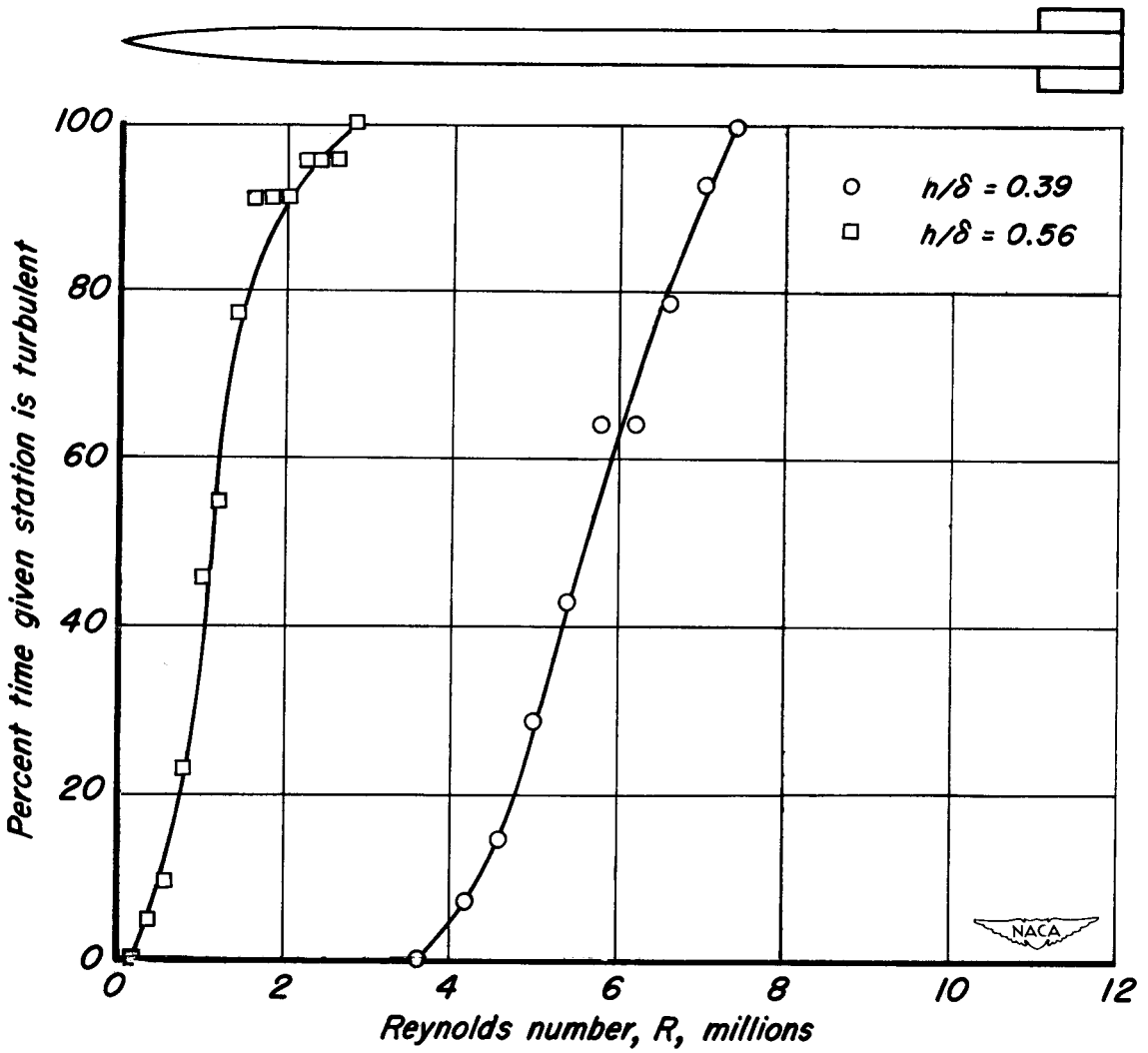

Figure 12.— Transition regions for coarse-thread models.

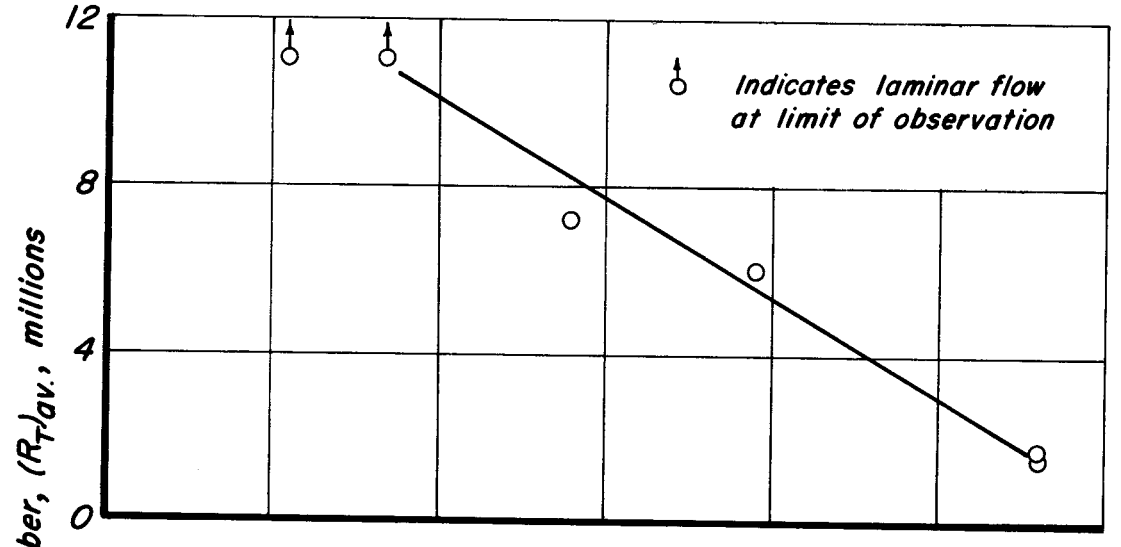

(a) Body length Reynolds number, R_l = 12 million

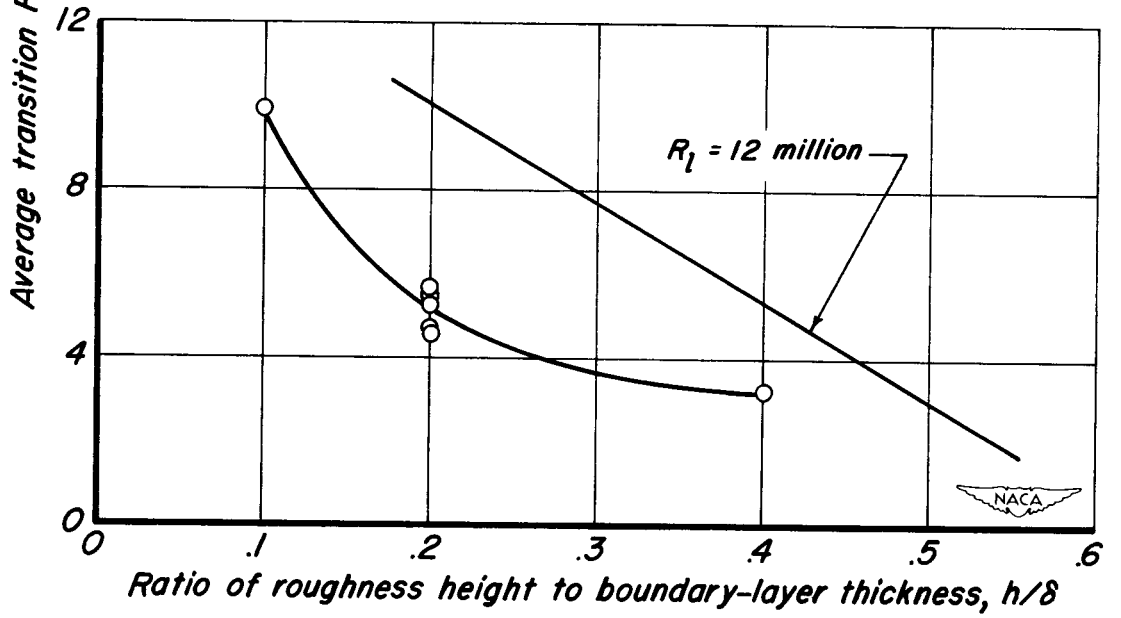

(b) Body length Reynolds number, R_l = 24 million

Figure 13.– Effect of thread height on transition Reynolds number at zero angle of attack.

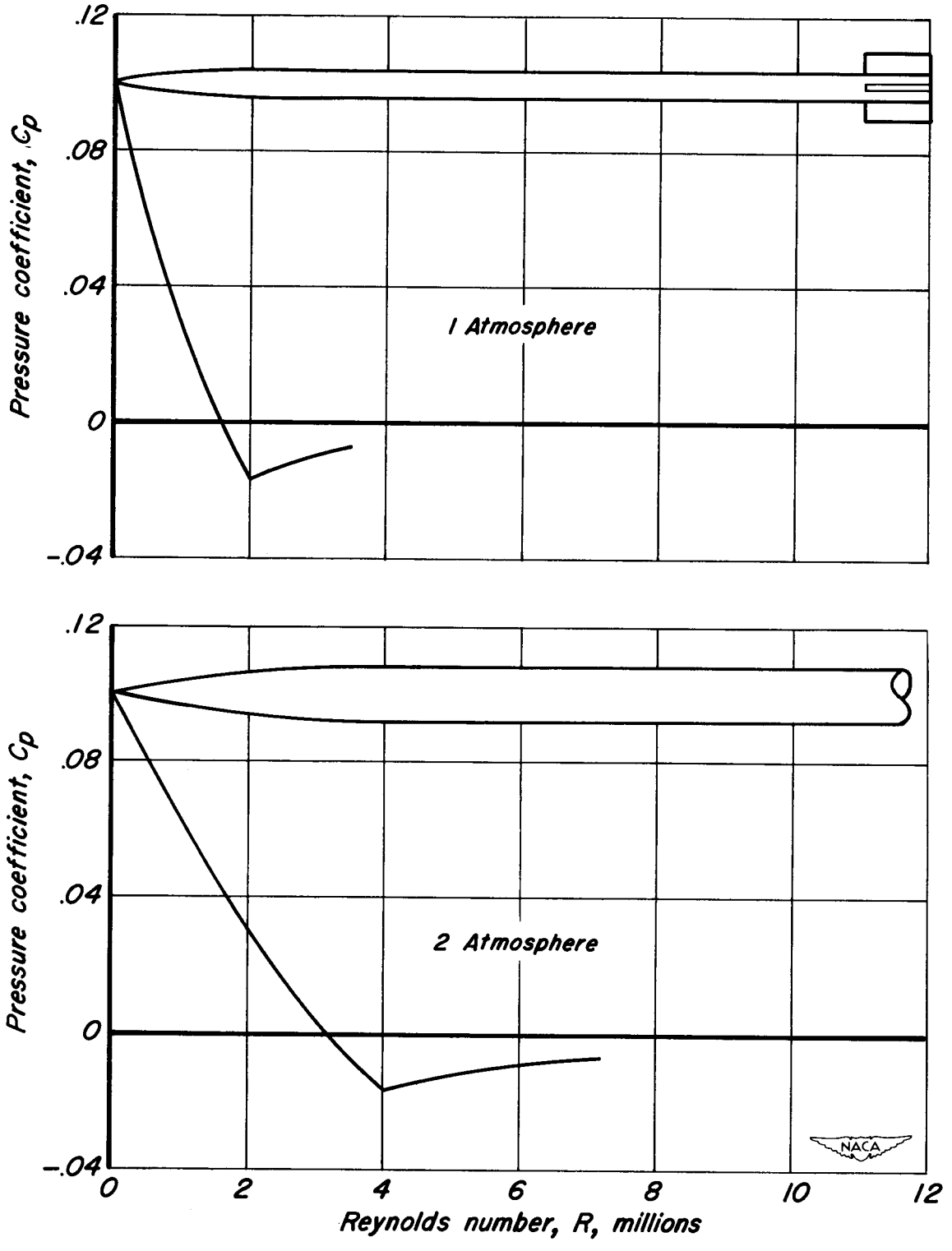

Figure 14.– Pressure coefficient as a function of Reynolds number at static pressures of 1 and 2 atmospheres.

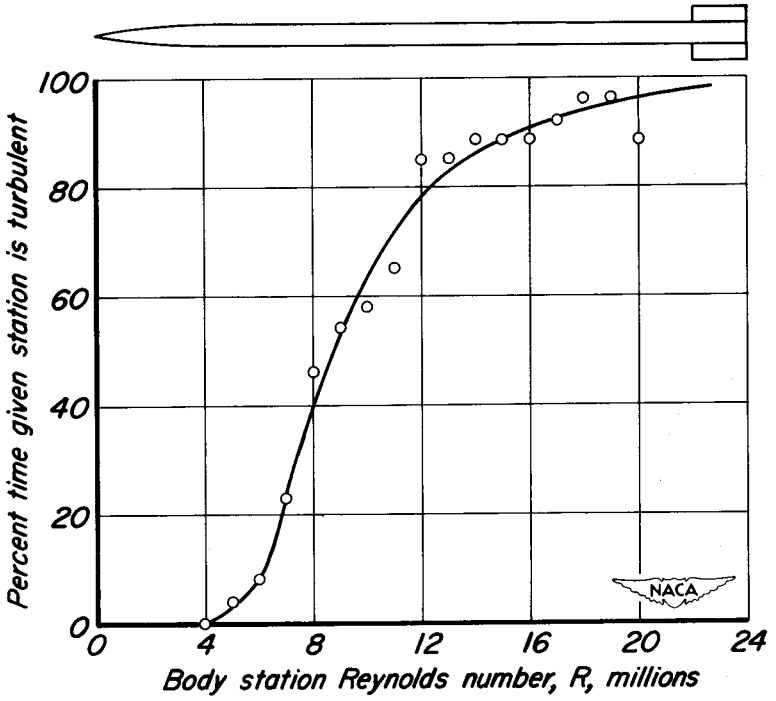

Figure 15.– Transition region for emery-polished models at 2 atmospheres static pressure.

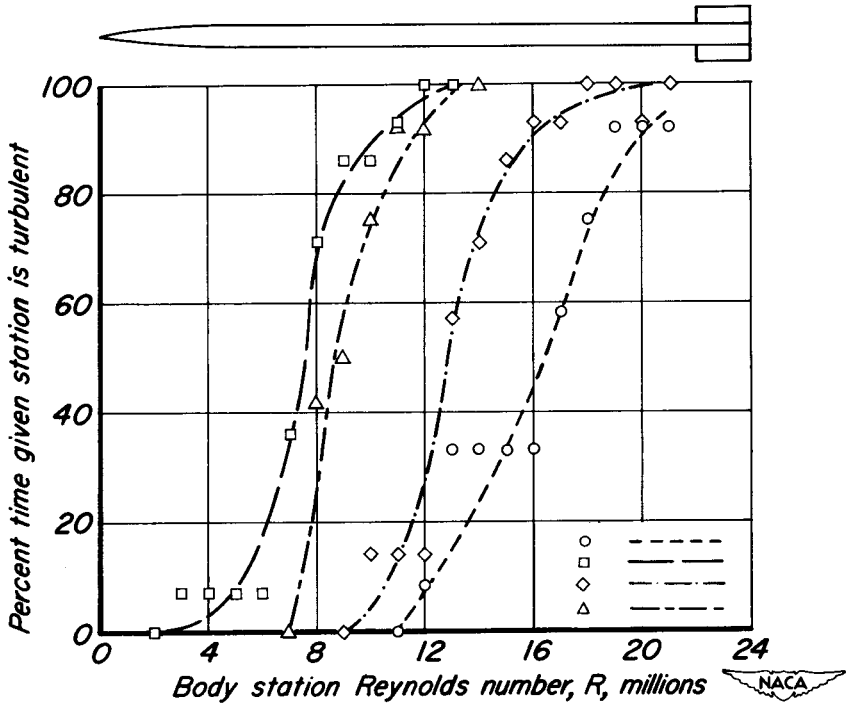

Figure 16.– Transition regions for four diamond-polished models at 2 atmospheres static pressure.

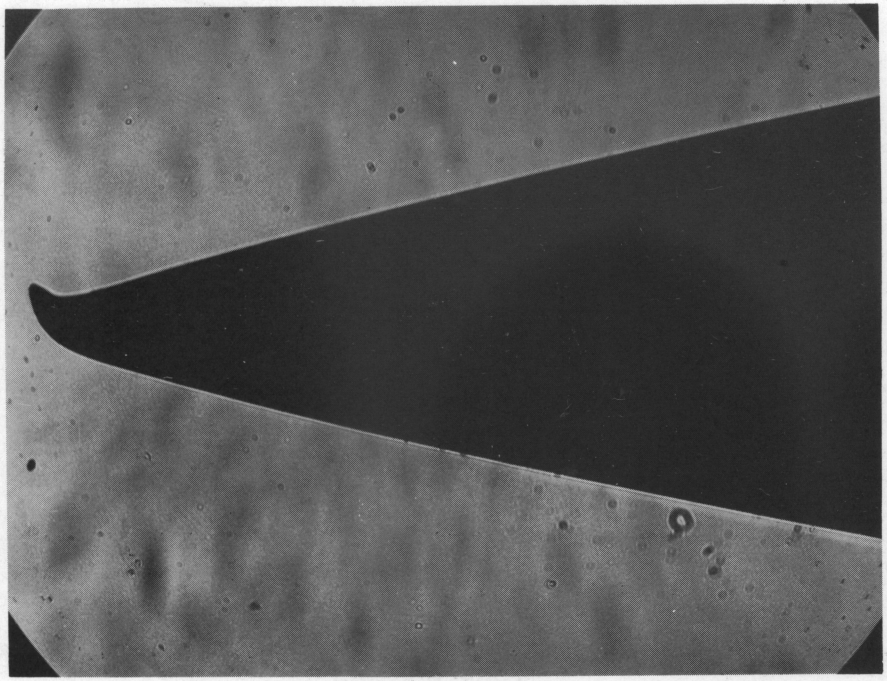

A-18626

Figure 17.- Model with tip hooked 0.003 inch off axis; X87.

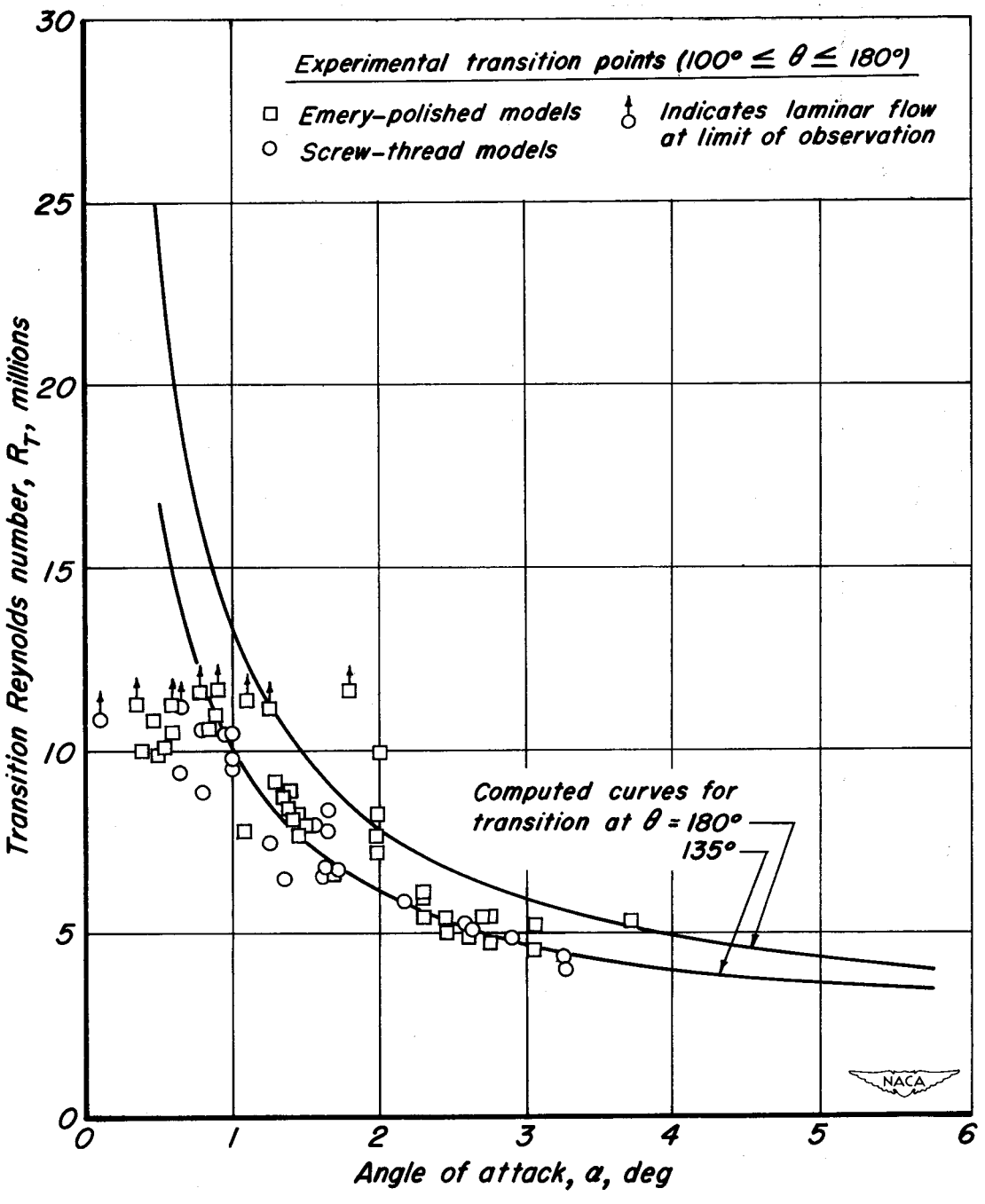

Figure 18.– Comparison of computed and experimental variations of R_T with α; R_t = 12 million.

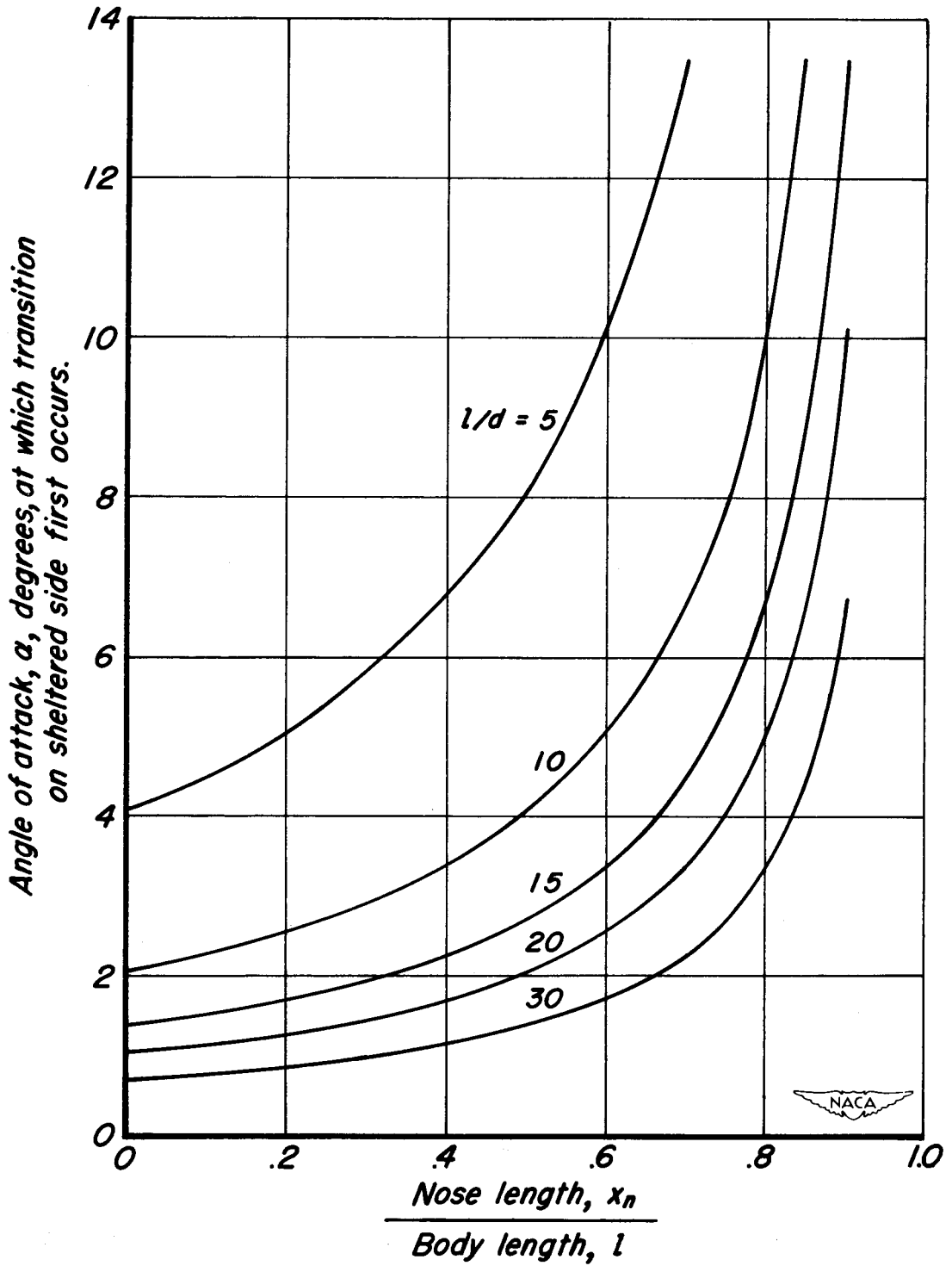

Figure 19.– The predicted effect of body geometry on sheltered-side transition.

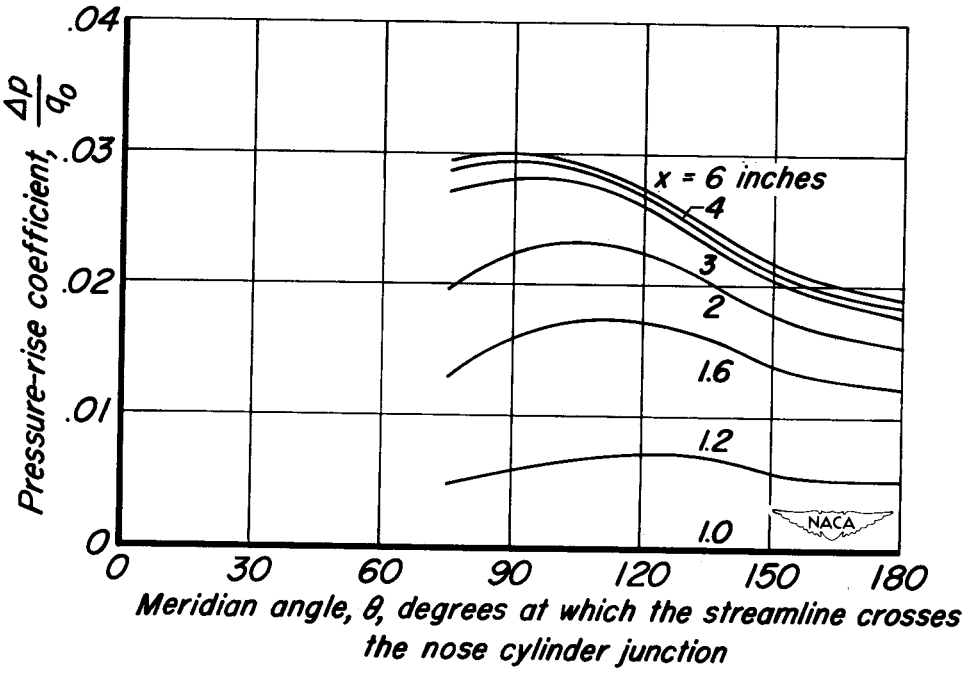

Figure 20.– Comparison of pressure rise along streamlines at various body stations; α = 3°.

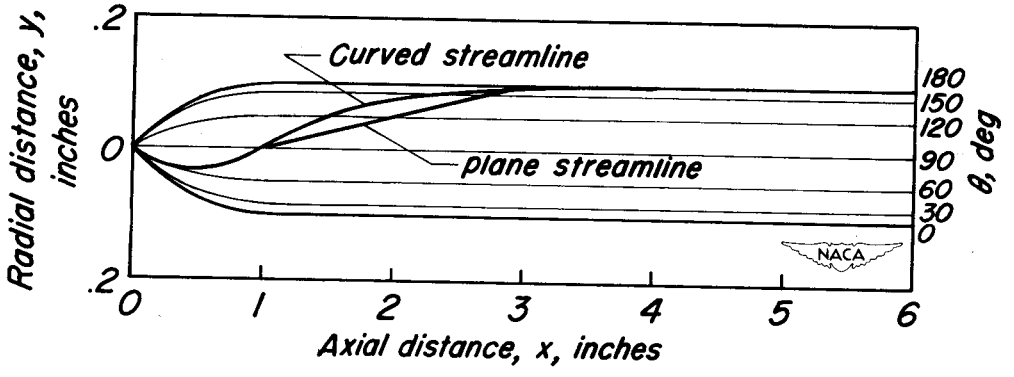

Figure 21.– Comparison of computed curved streamline with assumed plane path; α = 3°.

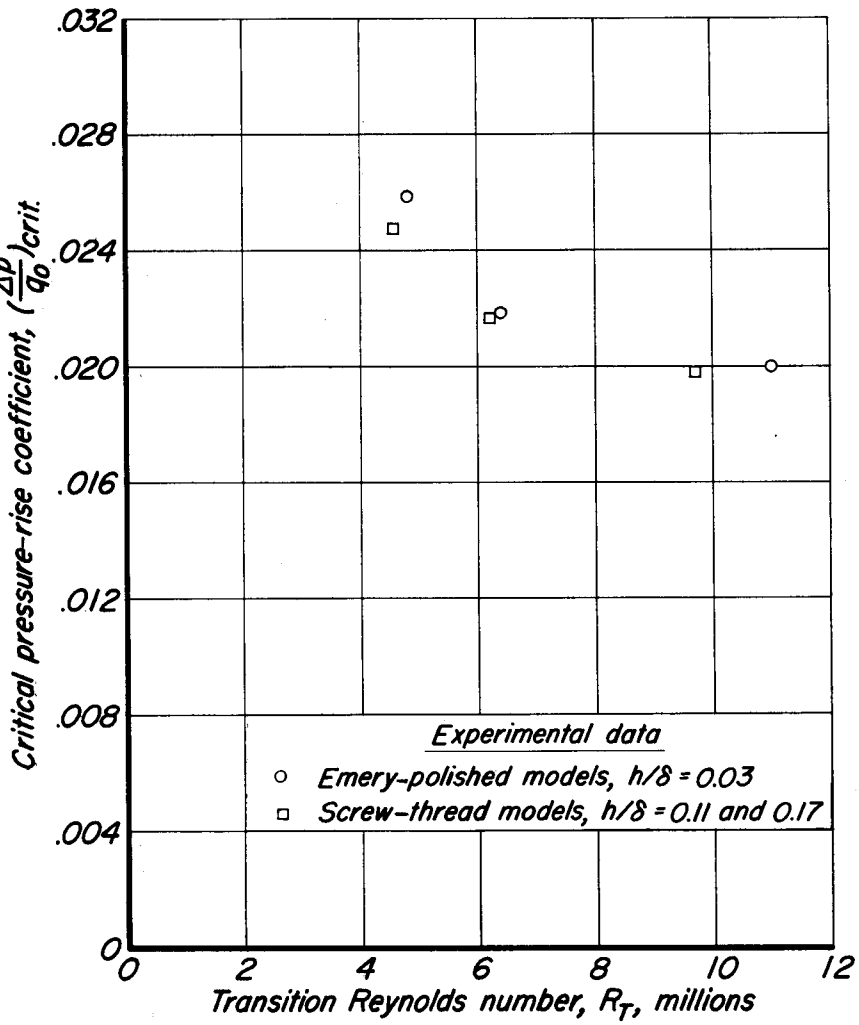

(a) Computed pressure-rise coefficients at which transition occurs.

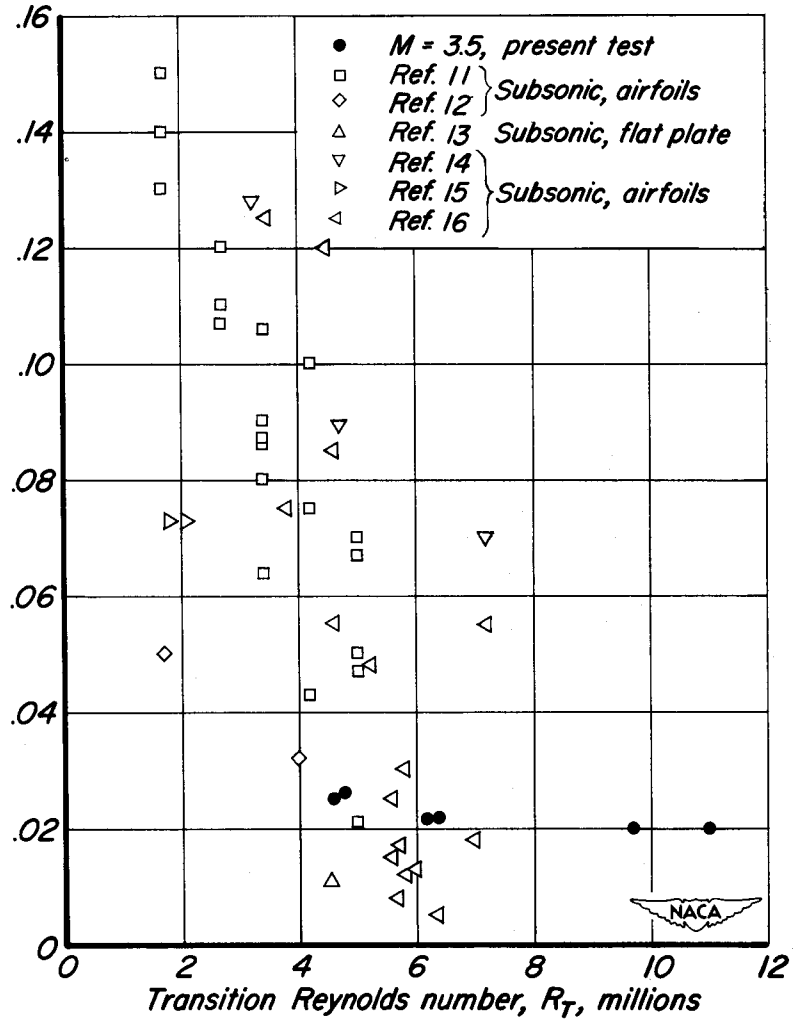

(b) Critical pressure-rise coefficients from subsonic data and present test.

Figure 22.– Critical pressure-rise coefficients as a function of Reynolds number of transition.

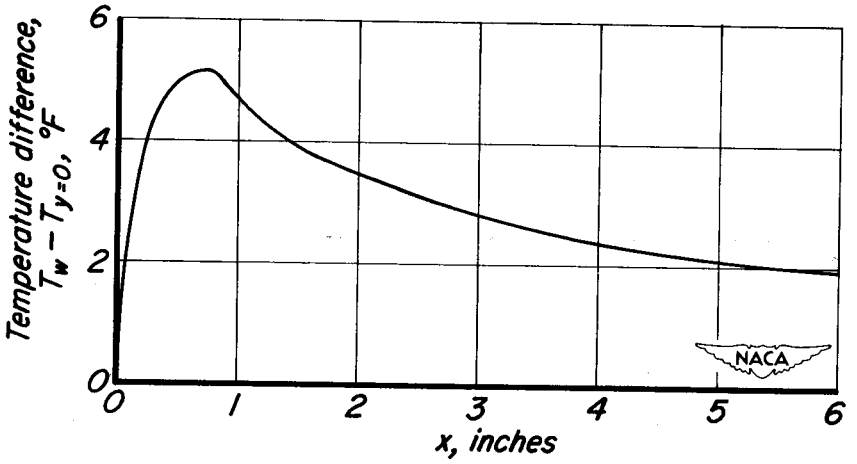

Figure 23.– Temperature difference between model surface and body center for transition model with laminar flow at M = 3.5, R = 12 million.

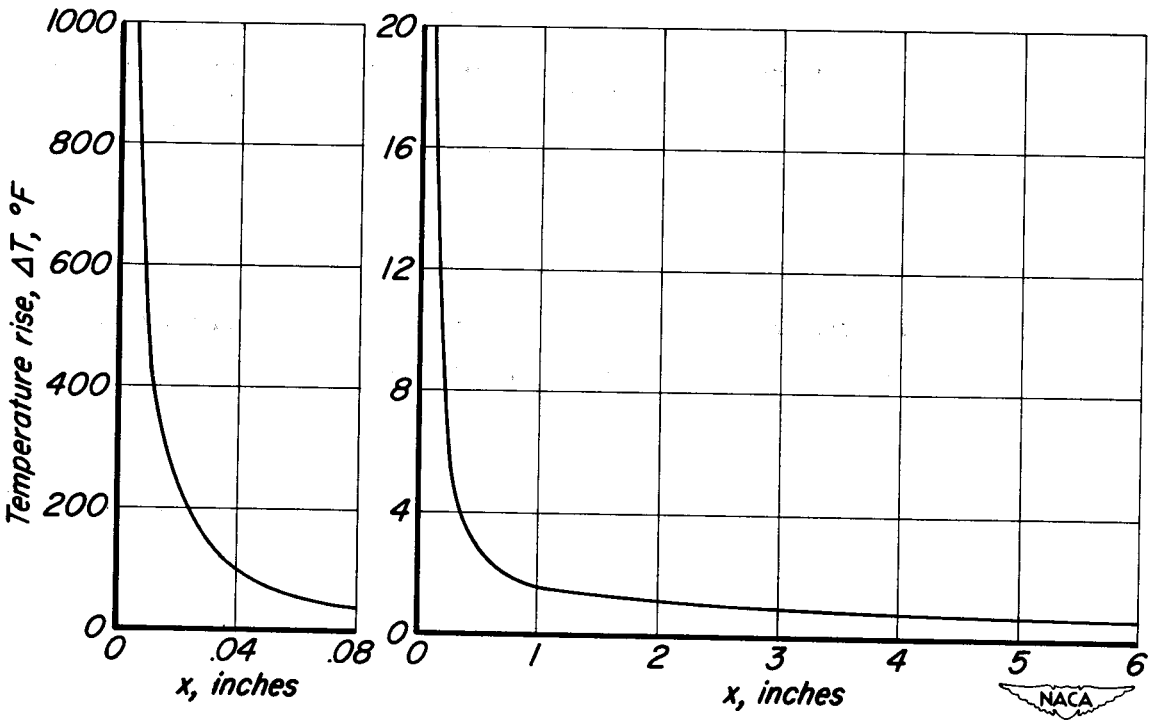

Figure 24.— Temperature rise of transition model for 50-foot flight at M = 3.5 and R_l = 12 million with laminar flow, no axial heat flow.

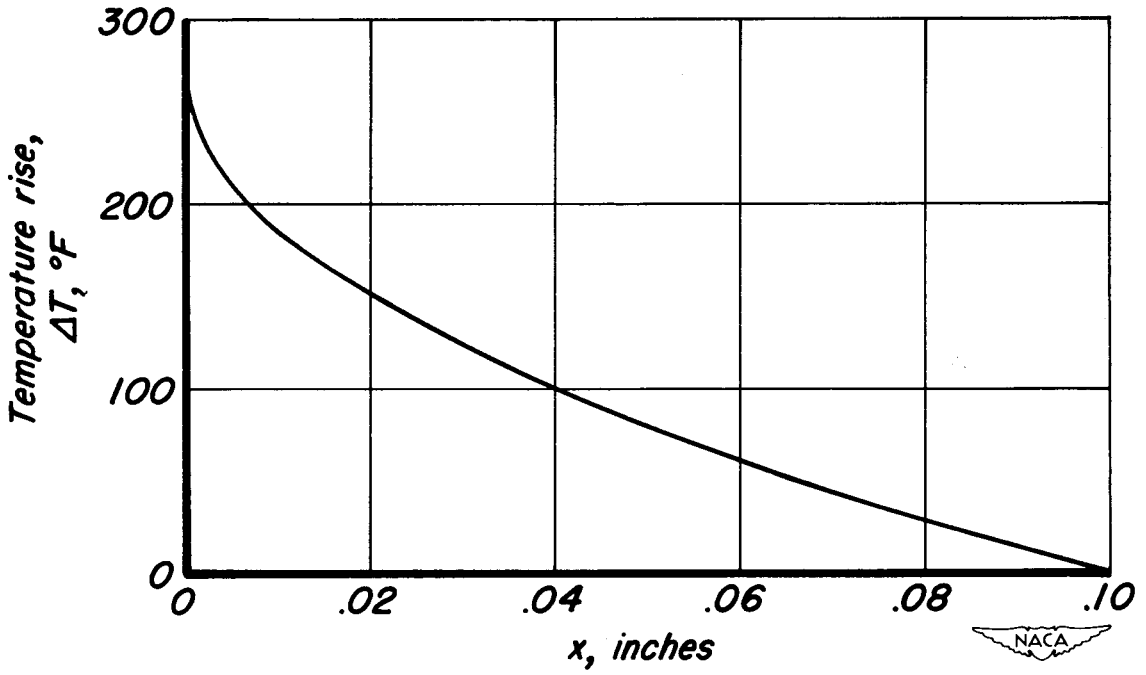

Figure 25. — Maximum possible axial temperature differences near tip in presence of axial heat flow.